Visual coding in the primary visual cortex: From single neuron to cortical ensemble

by

Feng Han

B.S. (Tsinghua University, Beijing) 2001

M.S. (Columbia University, New York) 2002

A dissertation submitted in partial satisfaction of the requirements for the degree of

Doctor of Philosophy

in

Vision Science

in the

GRADUATE DIVISION

of the

UNIVERSITY of CALIFORNIA, BERKELEY

Committee in charge:

Professor Yang Dan, Chair

Professor Stanley A. Klein

Professor Frederic Theunissen

Spring 2007

UMI Number: 3279624

UMI Microform 3279624

ProQuest Information and Learning Company
300 North Zeeb Road
P.O. Box 1346
Ann Arbor, MI 48106-1346

Visual coding in the primary visual cortex: From single neuron to cortical ensemble

Feng Han

Abstract

Visual coding in the primary visual cortex: From single neuron to cortical ensemble

by

Feng Han

Doctor of Philosophy in Vision Science

University of California, Berkeley

Professor Yang Dan, Chair

A fundamental question in sensory neuroscience is to understand how visual information is encoded and processed in the mammalian brain. In this thesis, I describe several electrophysiological experiments *in vivo* to investigate the mechanisms and plasticity of visual coding. Visual coding was explored at two levels: receptive field characterization of single cells and sensory experience-dependent plasticity in cortical ensemble.

In the first project, using single unit recording and computational analysis, I have characterized excitatory and suppressive subunits of neural receptive fields in awake primate. These subunits form a compact description of visual neurons, allowing prediction of the responses to arbitrary stimuli.

In the second project, neural responses to repetitive natural stimulation were investigated. I showed that repeated stimulation with movies of natural scenes induces a rapid improvement of response reliability, an effect largely absent with white noise and flashed bar stimuli. Furthermore the repeated movie stimulation also leaves a

memory trace in the subsequent spontaneous cortical activity, revealed by an increased similarity between the spontaneous firing patterns and the movie-evoked responses.

In a third project, by applying voltage-sensitive dye (VSD) imaging developed to measure activity of population of neurons simultaneously, I have examined whether and how spontaneous activity is modulated by sensory experience. VSD imaging of population activity in the rat visual cortex showed that following repetitive presentation of a given visual stimulus, spatial-temporal activity patterns resembling the evoked response appear more frequently in the spontaneous waves. Since correlated neuronal activity during waves is likely to be conducive to long-term synaptic modifications, wave-mediated reverberation may contribute to perceptual learning by consolidating the transient effect of recent sensory experience into long-lasting cortical modifications.

Table of Contents

Acknowledgements

I wish to acknowledge the guidance and assistance of my dissertation committee: Professor Stanley A. Klein, Frederic Theunissen, and Yang Dan. I particularly want to thank my supervisor, Yang Dan, for supporting me financially, academically and for being an extraordinary mentor throughout the course of my PhD. Yang has shown me a great deal of inspiration, and has nudged me along at the right times and in the right directions. I have learned a great deal from Yang about how to conduct science and most importantly how to become a real scientist.

I wish to thank my collaborators and friends in the Dan lab: Haishan Yao, Hongfeng Gao, Lei Shi, Natalia Caporale, Xiaodong Chen, Giao Hang and Chenyu Li for their advice and assistance with the experiments. And I am also grateful to the other members of the lab, Wenzhi Sun, Yuxi Fu, Jon Touryan, Gidon Felsen, Sachin Deshmukh, Uma Karmarkar, Mike and Jennie for their companionship and kind helps.

Lastly, I must give my most heartfelt appreciation to my husband, Jian Zhang, who loves and cares for me, and my mother and my father, for their unwavering support.

List of Figures

Chapter I. Introduction

Overview

A major challenge in neuroscience is to understand how visual information is encoded and processed in the mammalian brain. This question can be addressed on multiple levels. We can study how single neuron encodes sensory stimuli, extract relevant features, and then select an appropriate response. Linear and nonlinear computational techniques are used to analyze the responses to complex stimuli to understand the cortical circuitry underlying various response properties of visual neurons. We can also measure the activity of population of neurons simultaneously to characterize the spatial-temporal patterns of ensemble neural activity and their roles in visual coding. One fundamental organizing principle of cortical circuitry is plasticity. Visual stimulation can modify cortical circuitry and response properties on multiple time scales. For example, in contrast adaptation, exposure to high-contrast stimuli for seconds to minutes causes a reduction in response amplitude (Maffei, 1973) and changes in stimulus selectivity (Movshon, 1979) (Dragoi, 2000; Muller, 1999) of cortical neurons. Recent studies have also demonstrated shifts in cortical receptive field location and orientation tuning that depends on the relative timing of paired conditioning visual stimuli on the order of tens of milliseconds (Fu, 2002; Yao, 2001; Yao, 2004), consistent with spike-timing-dependent synaptic plasticity (STDP) (Markram, 1997; Bi, 1998). Together, these studies have demonstrated multiple forms of rapid plasticity in adult visual cortex.

The objective of my dissertation was to investigate the fundamental mechanisms underlying cortical function and plasticity of visual coding at two levels: from response

properties of single neuron to plasticity in cortical ensembles. To address those questions, two novel techniques have been applied: spike triggered covariance analysis and voltage sensitive dye imaging. Linear and nonlinear computational analysis (such as spike triggered average and spike triggered covariance) can be used to analyze neural responses to complex stimuli to understand the coding mechanism underlying various response properties of visual neurons. The emergence of many powerful functional imaging techniques (e.g. voltage-sensitive dye imaging, two-photon imaging etc.) enables us to examine neural activities in large cortical circuits over broad spatial and temporal scales.

Receptive field characterization

Forty years ago, Hubel and Wiesel first characterized the response properties of visual cortical neuron using simple geometric stimuli. Cortical cells are found to be tuned to a wide variety of parameters, including orientation and directed motion (Hubel & Wiesel, 1962). The emergence of such tuning is often conceptualized in terms of receptive fields (RFs), which are spatio-temporal functions that describe what best excites a neuron (Figure 1.1). Since then, continued focused effort has produced still greater insights into the characteristics of the receptive field. It has been widely accepted that simple cells compute linear summation of light intensities falling in the receptive fields (half-wave-rectified linear operators). Complex cells have been depicted as energy models (Alderson and Bergen 1985), constructed from the squared sum of the outputs of quadrature pairs of linear operators. The linear/energy model provides a simplified characterization of basic aspects of cell functions, and quantifications of receptive field properties in such model will provide us further insights into neural coding mechanisms.

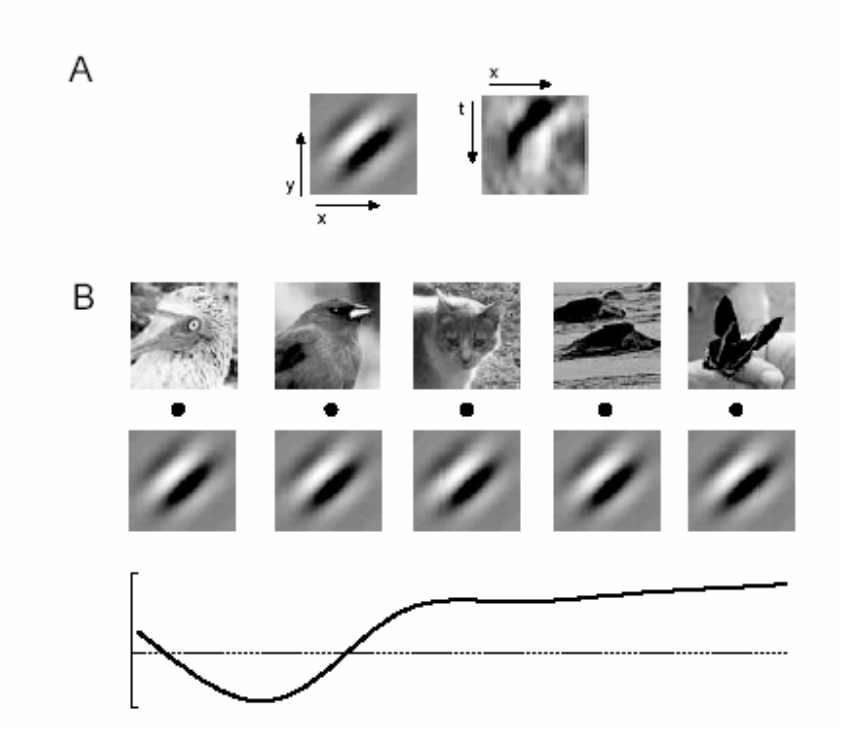

Figure 1.1: Visual Receptive Fields.
(A) Spatial (left) and spatiotemporal (right) examples of RFs.

(B) The response of the neuron to any given image can be predicted by computing the similarity of the stimulus to the RF, which, in the case of a spatial RF, is the dot product of the image with the RF (bottom plot). The resulting function often has to be further processed (e.g., by rectification) in order to predict the actual spike train. (Figure adapted from Dan Meliza 2006).

Characterizing neural receptive fields is an essential step to understand the functional relationship between environmental stimuli and neural response, therefore elucidate the *computation* being performed by the system. Receptive field properties of cortical neurons are typically determined by relative simple stimuli, such as light dots, bars and sinusoidal gratings by measuring the spike rate after stimulation based on the linearity assumption of neural responses. Those simple stimuli are easy to produce and

control, however they only cover a narrowly restricted range of stimulus space, therefore they cannot provide a complete description of neural response. A more comprehensive technique, white noise analysis, has been widely applied to characterize the neural system. Reverse correlation, one of the most commonly used forms of this method, computes the spike-triggered average (STA) by averaging stimulus blocks preceding each spike. Generally, STA can be interpreted as a linear representation of the receptive field, in which it represents the "excitatory" stimulus of the cell. In a nonlinear system analysis perspective, the system response function is fully characterized by a polynomial series of expansion, known as Wiener/Volterra series. If the system is truly linear, then STA provides a complete characterization. However, it is well known that neural responses are not linear. Thus the first tem of a Wiener/Volterra series as estimated with STA, will typically not provide a full description of neural response. Including more higher-order terms in the series expansion is more computational expansive and requires a substantial increase in the amount of experimental data. Fortunately, under certain conditions of the stimulus distribution and nonlinearity, STA is able to characterize a linear fitting of the neural response function [Chichilnisky 2001]. Specifically, STA describes an unbiased estimation of the linear kernel of a linear-nonlinear-Poisson (LNP) model which is a generally used as a linear model of simple cell.

Estimating the receptive fields for complex cells poses more challenges to STA. Complex cell is usually described as "energy model". Not only does this model use two linear filters, but the symmetry of the rectifying nonlinearity means that the STA will be zero, thus providing no information about the linear stage of the model. In this particular case, a variety of second-order interaction analyses have been developed to recover the

two filters (e.g., Emerson *et al.*, 1987; Szulborski & Palmer, 1990; Emerson *et al.*, 1992). An extension of STA method, known as spike-triggered covariance (STC) method has been shown to be highly effective in analyzing receptive fields for complex cells (Felsen et al., 2005; Touryan et al., 2005; Touryan et al., 2002 and Rust et al., 2005). It is the STC analysis that is the focus of the first project in this thesis. And this method will be detailed in the section of spike-triggered covariance analysis in this chapter.

Experience-dependent plasticity in adult visual cortex

Experience-dependent synaptic plasticity is a fundamental organizing principle for neural system. Particularly in visual cortex, visual stimulation can modify cortical circuitry and response properties on multiple time scales. For example, in contrast adaptation, exposure to high-contrast stimuli for seconds to minutes causes a reduction in response amplitude (Maffei, 1973) and changes in stimulus selectivity (Movshon, 1979) (Dragoi, 2000; Muller, 1999) of cortical neurons. These changes may be due to reduced neuronal excitability (Carandini, 1997; Sanchez-Vives, 2000) or short-term synaptic depression (Chance, 1998).

Although developmental refinement of cortical circuitry is most evident in young animals, experience-dependent improvement of visual cortical function can occur throughout the lifetime of the animal, as revealed by studies of perceptual learning in adults (Fahle, 2002) (Furmanski, 2004) (Schoups, 2001) (Crist, 2001)(Li, 2004).

On the time scale of several minutes, the receptive field structures of individual cells in the mature cat visual cortex have been shown to be able to adapt in different contexts. Associated co-stimulation within the receptive field and in a non-responsive surround region causes an expansion of the receptive field into the non-responsive

surround within minutes (Eysel, 1998). Such expansion of the receptive field into the co-stimulated surround areas could be accounted for by Hebbian synaptic plasticity (Hebb, 1949).

Recent studies have also demonstrated shifts in cortical receptive field location and orientation tuning which depend on the relative timing of paired conditioning visual stimuli on the order of tens of milliseconds (Fu, 2002; Yao, 2001; Yao, 2004), consistent with spike-timing-dependent synaptic plasticity (STDP) (Markram, 1997; Bi, 1998). In adult cat primary visual cortex, pairing of visual stimuli at two orientations induced a shift in orientation tuning, with the direction of the shift depending on the temporal order of the stimulus pair (Yao and Dan, 2001). Similar conditioning also induced a shift in the perception of orientation by human subjects. Such shifts induced by monocular conditioning show an inter-ocular transfer; therefore they are likely due to circuit modifications at the cortical level, where visual signals from the two eyes are converged. In addition to the orientation domain, stimulus timing-dependent cortical modification has also been demonstrated in the space domain (Fu et al., 2002). Flashing asynchronous visual stimuli in two adjacent retinal regions were found to control the relative spike timing of two groups of cortical neurons with a precision of tens of milliseconds. Asynchronous flashes induced modifications of intra-cortical connections (as revealed by cross-correlation analysis) and shifts in receptive fields. These changes depended on the temporal order and interval between the stimuli, consistent with STDP of intra-cortical connections. Similar to the modifications in cat V1, asynchronous conditioning also induced shifts in perceived object position by human subjects.

Together, these studies have demonstrated multiple forms of rapid plasticity in

adult visual cortex. It is therefore critical to understand the impacts of these mechanisms on cortical states and how they enhance visual processing which will be an important step in understanding the neural basis of higher cognitive functions such as learning and memory.

Spike triggered covariance analysis

An extension of STA method, known as spike-triggered covariance (STC) method has been shown to be able to describe the neural response of multi-filter LNP model such as energy model. STC comes from a natural extension of STA by introducing the second-order term in Weiner series, which describes the response function by all the pair wise products of stimulus vector (covariance matrix). Compared with STA, which is seeking for a single dimension reflecting difference of the mean firing rate between spike-triggered ensemble and raw stimulus ensemble, STC is seeking for a set of directions in the stimulus space along which the variance of spike-triggered ensemble differs from that of the raw stimulus ensemble.

In general, if certain features in the visual stimuli affect the firing probability of the cell, the spike-triggered stimulus ensemble should exhibit a different probability distribution from the entire stimulus ensemble (see Fig. 1.2*B*; compare the distribution of the *filled circles* and the distribution of all of the *circles*). Although a change in the probability distribution can be reflected in a change in the first-order (mean), second-order (variance), or higher-order moments, the correlation analysis aims to identify features with changed variance. Because PCA results in a set of components with their variance ranking from the highest to the lowest, it is ideally suited for the identification of

features with outstanding variance. Practically, identification of relevant features was achieved by finding eigenvalues of the spike-triggered correlation matrix that were significantly different from the eigenvalues of the control correlation matrix (computed by randomly sampling the entire stimulus ensemble). For example, assuming the pattern in the stimulus ensemble consisted of P parameters. The spike-triggered correlation matrix, [*C*m,n] (*m*, *n* _ 1, 2, . . . , P) was computed as follows: $C_{m,n} = \frac{1}{N}\sum_{i=1}^{N} S_m(i)S_n(i)$,

where *S*m(*i*) and *S*n(*i*) are the *m*th and *n*th parameters of the stimulus pattern preceding the *i*th spike, respectively, and *N* is the total number of spikes in the response. The resulting matrix is closely related to the second-order Wiener kernel (Wiener, 1958; Marmeralis and Marmeralis, 1978) of the neuron. Eigenvalues and eigenvectors of this spike-triggered correlation matrix were then computed. The rank of eigenvalue of spike-triggered correlation matrix reflects the rank of variance of the corresponding stimulus dimensions. In particular, an increase in variance represents the excitatory dimensions of the stimulus and a decrease in variance represents the inhibitory dimensions of the stimulus. Finally, it is important to keep in mind that this method does not necessarily identify all of the features that affect the responses of the neuron, especially those that contribute weakly to the response.

The STC analysis can reveal stimulus features that drive the neuron in a contrast-dependent but polarity invariant manner and recover both excitatory and suppressive subunits of a neural response function. It has proved highly effective in the analysis of complex cell RF subunits in both cat (Felsen et al., 2005; Touryan et al., 2005; Touryan et al., 2002) and monkey (Rust et al., 2005) V1.

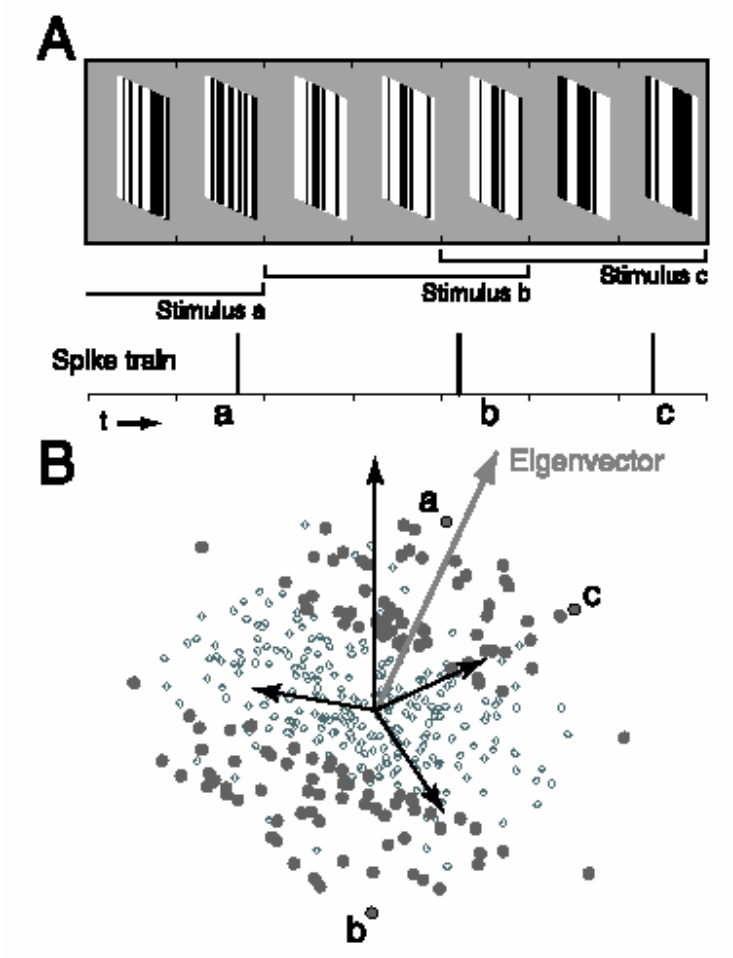

Figure 1.2. Illustration of a spike-triggered correlation analysis.

A, Spatiotemporal random-bar stimuli (top) and the spike train response (bottom). Each bracket indicates a spatiotemporal stimulus pattern preceding a spike (for actual analysis, each pattern contained 16 rather than 3 frames).

B, Schematic representation of the spike-triggered stimulus ensemble (filled circles) and the entire stimulus ensemble (open and filled circles) in a multidimensional parameter space. Each axis (black arrows) represents luminance at a particular bar position and time frame, and each point represents a stimulus pattern. Note that the actual stimulus ensemble is represented in a 256-dimensional space (16 frames by 16 bars). a–c indicate stimulus patterns shown in A. The gray arrow indicates an eigenvector of the spike-

triggered ensemble with its eigenvalue (variance) greater than the eigenvalues of the entire ensemble. (Figure adapted from Touryan 2002)

Voltage-sensitive dye imaging

Properties of cortical networks that are not reflected in the electrical activity of single neurons can be revealed and subsequently fully understood only by studying the activity in neuronal populations. Voltage-sensitive dyes imaging (VSDI) can be used to visualize electrical activity in population of neurons at a high spatial and temporal resolution. The dye molecules bind to the external surface of cell membranes and transform changes in membrane potential into optical signals.

Voltage-sensitive dyes

A typical dye is a long conjugated molecule consisting of one hydrophobic tail at one end and a fixed charge at the other hydrophilic end as shown in fig 1.3 top. The hydrophobic tail anchors the dye in the lipid bi-layer, while the charged hydrophilic end tends to prevent the dye from crossing the neuronal membranes freely. In addition, the large dipole makes the dye sensitive to the changes in the electric field across the neuronal membrane during activity. The dye's sensitivity to voltage changes can be explained by several possible mechanisms: a direct electro-chromic effect or the motion of the molecule in and out of the membrane as a function of the changing electric field across the membrane, affecting its optical properties such as the color or fluorescence quantum yield.

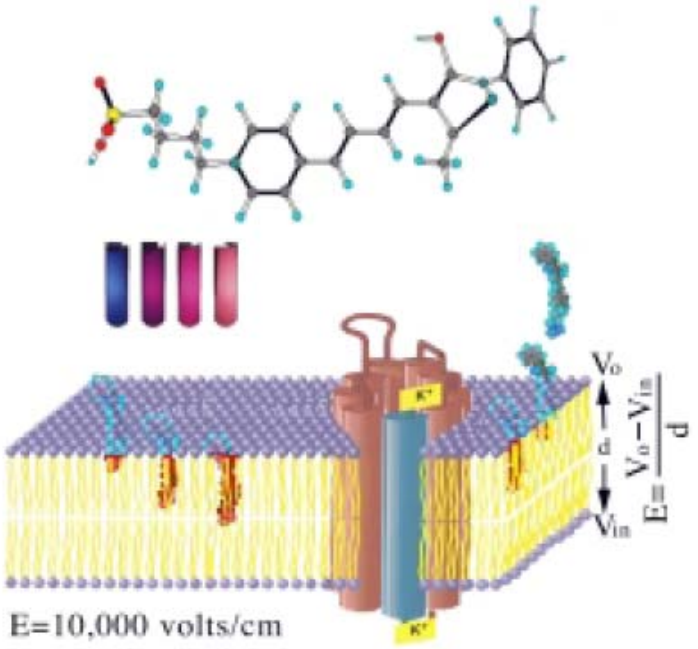

Figure 1.3 Voltage-sensitive dyes. Top**:** The chemical structure of a voltage-sensitive dye RH 795. The 4 test tubes below the dye structure contain another voltage-sensitive dye dissolved in 4 different solvents of very different polarity. The large changes in its color indicate that this dye is sensitive to its microenvironment. Bottom: Schematic illustration of the dye interactions with the lipid bi-layer, depicting one out of many possible mechanisms responsible for a dye ability to transduce the membrane potential change into an optical signal. Dye molecules not bound to the lipid bi layer are not fluorescent (depicted in blue). Once the dye binds it becomes fluorescent (red). The intensity of the fluorescence depends on the extent that the dye hydrophobic portion interacts with the hydrophobic portion of the bi-layer. Since the dye is both charged and polar, it may change its interaction with the bi-layer, depending on the electric field across the bi-layer. An action potential gives rise to a change in electric field of ~ 20,000 Volts across the bi-layer. Such a large electric field change can also induce an electro-chromic effect even if the dye does not move during an action potential. (Figure adapted from *www.opticalimaging.com*)

What does the dye measure in vivo?

Direct intracellular recordings, combined with VSDI resolved controversies about what the dye signal reflects during in vivo measurements. The results established that the dye signal reflects changes in membrane potential and follows an identical time course as intracellular electrical recordings. The VSD signal is linearly related to the stained membrane area, and most of the dye signal originates from cortical dendrites rather than cell bodies, because their membrane areas are orders of magnitude larger than that of neuronal soma (Grinvald et al., 1984; Grinvald et al., 1982; Orbach and Cohen., 1983; Orbach et al., 1985). Therefore, the VSD signal *in vivo* mainly reflects dendritic activity. Nevertheless, VSDI has provided high-resolution maps, which correspond to cortical columns, and offer a spatial resolution better than 50 μm. The VSD response time is in microseconds and the ultimate spatial resolution of VSDI is about 0.5 μm — it is limited by optics and light scattering.

Imaging apparatus

The apparatus required for VSD imaging *in vivo* includes: (a) A fast camera is required (2000Hz to 300Hz) to record optical signals, (b) a macroscope with epi-illumination option with appropriate excitation filter and a dichroic mirror is required and (c) Computer and elaborate software for data acquisition, display and preliminary online analysis should be put in place. A scheme of the apparatus is shown in Figure 1.4.

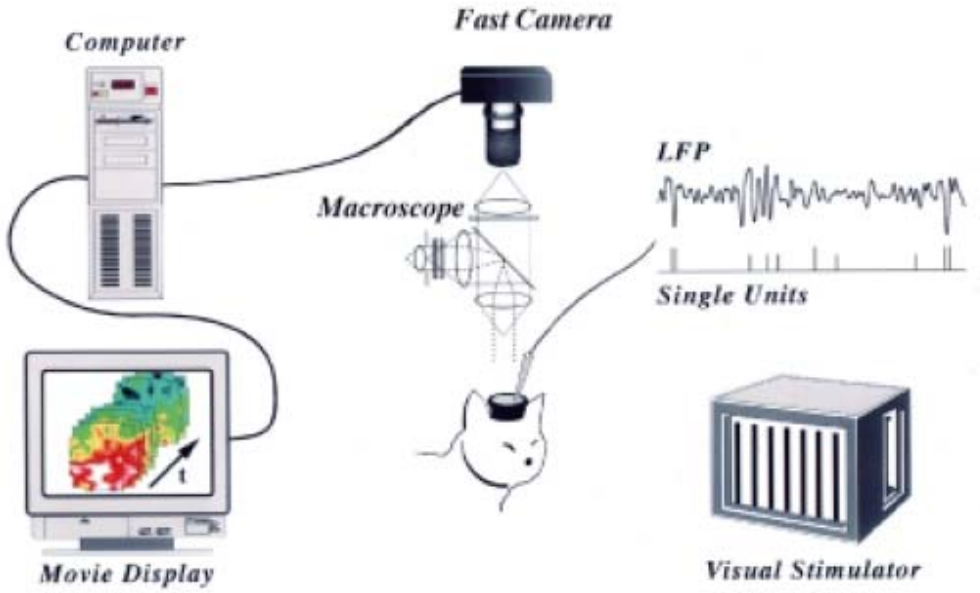

Figure 1.4 The real-time optical imaging system. The exposed cortex was stained for 2 hours by topical application of a voltage-sensitive dye. An image of a 2 to 5 mm large square area of visual cortex was projected onto a fast camera with the aid of a macroscope. Computer controlled visual stimuli were presented on a video monitor. Images of the cortical fluorescence were taken at 10000Hz. The output of the fast camera was displayed in slow motion on an RGB monitor using either gray scale, color coded or surface plot images. Local field potentials, multi- or single unit activity or intracellular recording were performed simultaneously. (Figure adapted from *www.opticalimaging.com*)

Signal to noise ratio

VSD signals tend to be very small. And when the fluorescence signals are small, the activity-dependent (dye unrelated) light-scattering or slow hemodynamic intrinsic signals from the preparation may distort the voltage-sensitive optical signals. A solution to this problem is to subtract the light-scattering signals from the total optical response by measuring it independently in the proper way. This task may not be easy. The magnitude

of the distortion of the "voltage signals" depends on the relative size of the intrinsic signal and the dye signal at the wavelength used for the imaging. With the improvement of blue dyes (Shoham et al., 1999), which largely avoid the hemodynamic wavelength, sensory evoked activity can be observed from mammalian cortex *in vivo* with high signal-to-noise ratio (Derdikman 2003; Petersen 2003; Grinvald and Hildesheim, 2004; Ferezou, 2006).

Limitations and side effects

Two major factors limit the imaging duration of VSDI experiments. One is photodynamic damage. The dye molecules, in the presence of intense illumination, sensitize the formation of reactive singlet oxygen. These reactive radicals attack membrane components and damage the neurons. With current dyes, the imaging session is limited to approximately 20-60 minutes of continuous illumination before significant damage occurs. Cells can repair damage to their membrane, provided that the damage is not too large. A preliminary observation suggested that brief exposure to bright light, followed by a long inter-stimulus interval (e.g., 30 seconds) reduces the accumulated damage, in signal-averaging experiments, to a level that is much lower than that observed for continuous illumination (methodology from *www.opticalimaging.com*). Dye bleaching may affect the time course of the optical signals, especially in fluorescence measurements if an intense light source was used. Several offline correction procedures can be applied. For example, a subtraction procedure, has even described as effective (Grinvald et al, 1984, 1994). Bleaching during the optical measurement also limits the duration of the measurement. Thus, to minimize bleaching, the exposure time of the preparation to light should be reduced to a minimum. If the bleaching reduces the signal

size prior to the onset of photodynamic damage, then the preparation can be restained and the cortex can be imaged again.

Applications in vivo

Because of its high resolution in both space and time domains, VSDI has been used to investigate fundamental questions relating to visual processing, ongoing activity and perception. One application is to visualize the dynamics of orientation selectivity in the millisecond time domain. Technical advances in VSDI have made it possible to obtain time-series of single condition orientation maps millisecond by millisecond, at sub-columnar resolution (Sharon 2002).

VSDI is highly sensitive to subthreshold activity, and it is therefore suitable for exploring the underlying neural mechanisms of visual illusions. VSDI was used to image the responses in the cat visual cortex to a well-known motion illusion described almost a century ago by Gestalt psychologists, in which a stationary square followed immediately by a long stationary bar produces the illusion that the bar ‘sweeps’ away from the square. The dynamic activity patterns of the cortex to a square flashed shortly before a bar resembled those produced by the real movement in the visual stimulation (Jancke 2004). These findings emphasize the effect of spatio-temporal patterns of subthreshold synaptic potentials on cortical processing and perception.

VSDI has also been used to study ongoing cortical activity, which occurs in the absence of sensory input. Although such activity is often thought of as 'noise', VSDI revealed that it can be coherent and of large amplitude. As such fluctuations will affect how far neurons are from their firing threshold, ongoing activity could shape neuronal responses to sensory stimuli. One example is that study found that response variability to

the same stimulus could be accounted for by the spatio-temporal patterns of ongoing activity, reflecting the dynamic states of neocortical networks. The central finding in the initial studies of ongoing activity, using VSDI without signal averaging, was that despite this large variability, the evoked responses in single trials could be predicted precisely by taking into account the preceding ongoing activity (Arieli 1996).

Conclusion

Properties of neural receptive fields (RFs) and activity-dependent visual plasticity are two fundamental aspects in understanding the mechanisms and functions of visual coding. It is essential to reveal those properties in both single unit level and cortical networks. VSDI is ideal for studying spatial-temporal activity patterns of population of neurons. Therefore combining single unit recording and VSDI might provide a multi-scale understanding of visual coding.

The primary discoveries of the experiments reported in this thesis detail several extensions in studying receptive fields and visual plasticity for understanding visual coding in the adult mammalian cortex. The experiments described in Chapter II revealed the structures of receptive fields in the awake monkey V1. Characterizing neural receptive fields is believed to be an essential step in understanding visual processing. We found multiple excitatory and suppressive subunits including one or two dominant excitatory subunits as described by the standard model for most of the cells. Compared to the dominant subunits, the additional subunits although with relatively smaller weights, contribute to several important neural response properties, such as response invariance to stimulus position, orientation and spatial frequency and cross orientation suppression.

Together, the excitatory and suppressive subunits form a compact description of neuronal RFs in awake monkey V1, allowing prediction of the responses to arbitrary stimuli.

Chapter III demonstrates a form of rapid plasticity in cat visual cortex induced by repeated natural stimulation. We show that repetitive exposure with movies of natural scenes induces a rapid improvement of response reliability, an effect largely absent with white noise and flashed bar stimuli. The improved reliability can be accounted for by a selective increase in spiking evoked by preferred stimuli, and the magnitude of improvement depends on the sparseness of the response. The increase in reliability persists for at least several minutes in the absence of further movie stimulation. During this period, there is detectable reverberation of the movie-evoked responses in the spontaneous spiking activity. Thus, repeated exposure to natural stimuli not only induces a rapid improvement of cortical response reliability, but also leaves a "memory trace" in subsequent spontaneous activity.

In chapter IV, we specifically investigated whether and how spontaneous activity is modulated by sensory experience in neural circuit using voltage-sensitive dye imaging. We report that visually evoked activity reverberates in subsequent spontaneous cortical waves. Voltage-sensitive dye imaging of population activity in the rat visual cortex showed that following repetitive presentation of a given visual stimulus, spatiotemporal activity patterns resembling the evoked response appear more frequently in the spontaneous waves. This effect is specific to the cortical response pattern evoked by the repeated stimulus, and it persists for several minutes. Such "reverberation" of visually evoked responses may contribute to transient perceptual memory. Furthermore, since correlated neuronal activity during waves is likely to be conducive to long-term synaptic

modifications, wave-mediated reverberation may contribute to perceptual learning by consolidating the transient effect of recent sensory experience into long-lasting cortical modifications.

Reference

Adelson, E. H., and Bergen, J. R. Spatiotemporal energy models for the perception of motion. J Opt Soc Am A *2*, 284-299. (1985).

Arieli, A., Sterkin, A., Grinvald, A. & Aertsen, A. Dynamics of ongoing activity: explanation of the large variability in evoked cortical responses. Science 273, 1868-1871 (1996).

Bi, G.Q. and Poo, M.M., Synaptic modifications in cultured hippocampal neurons: dependence on spike timing, synaptic strength, and postsynaptic cell type. *J. Neurosci.* **18**, pp. 10464–10472. (1998)

Cohen, L. B. & Lesher, S. Optical monitoring of membrane potential: methods of multisite optical measurement. *Soc. Gen. Physiol. Ser*. **40**, 71–99 (1986).

Dragoi V, Sharma J, and Sur M. Adaptation-induced plasticity of orientation tuning in adult visual cortex. *Neuron.* 28, 287-298 (2000)

Felsen, G., Touryan, J., Han, F., and Dan, Y. Cortical sensitivity to visual features in natural scenes. PLoS Biol *3*, e342. (2005).

Ferezou, I., Bolea, S. & Petersen, C. C. Visualizing the cortical representation of whisker touch: voltage-sensitive dye imaging in freely moving mice. Neuron 50, 617-29 (2006).

Fu, Y.X., Djupsund, K., Gao, H., Hayden, B., Shen, K. and Dan, Y., Temporal specificity in the cortical plasticity of visual space representation. *Science* **296**, pp. 1999–2003.(2002)

Fu, Y.X., Shen, Y., Gao, H. and Dan, Y., Asymmetry in visual cortical circuits underlying motion-induced perceptual mislocalization. *J. Neurosci.* **24**, pp. 2165–2171. (2004)

Grinvald, A., Manker, A. & Segal, M. Visualization of the spread of electrical activity in rat hippocampal slices by voltage sensitive optical probes. *J. Physiol.* **333**, 269–291 (1982).

Grinvald, A. Real time optical imaging of neuronal activity: from single growth cones to the intact brain. *Trends Neurosci*. **7**, 143–150 (1984).

Grinvald, A. & Hildesheim, R.VSDI: a new era in functional imaging of cortical dynamics. Nature Rev. Neurosci. Vol 5 (2004)

J. A. Movshon and P. Lennie. Pattern selective adaptation in striate cortical neurones. *Nature* **278**, 850-852 (1979)

Jancke, D., Chavane, F., Naaman, S., & Grinvald, A., Imaging cortical correlates of illusion in early visual cortex. *Nature*, March 25, vol 428: 423-426 (2004)

Maffei, L., Fiorentini, A., and Bisti, S. Neural correlate of perceptual adaptation to gratings. Science *182*, 1036-1038. (1973).

Matteo Carandini, David J. Heeger, J. Anthony Movshon, Linearity and Normalization in Simple Cells of the Macaque Primary Visual Cortex. The Journal of Neuroscience, November 1, *17*(21):8621–8644 (1997)

Malonek, D. & Grinvald, A. Interactions between electrical activity and cortical microcirculation revealed by imaging spectroscopy: implications for functional brain mapping. *Science***272**, 551–554 (1996).

Markram, H., Lubke, J., Frotscher, M. and Sakmann, B., Regulation of synaptic efficacy

by coincidence of postsynaptic APs and EPSPs. *Science* **275**, pp. 213–215. (1997)

Petersen, C. C., Hahn, T. T., Mehta, M., Grinvald, A. & Sakmann, B. Interaction of sensory responses with spontaneous depolarization in layer 2/3 barrel cortex. Proc Natl Acad Sci U S A 100, 13638-43 (2003).

Rust, N. C., Schwartz, O., Movshon, J. A., and Simoncelli, E. P. Spatiotemporal elements of macaque v1 receptive fields. Neuron *46*, 945-956. (2005).

Sanchez-Vives, M.V. and McCormick, D.A. Cellular and network mechanisms of rhythmic recurrent activity in neocortex. Nature Neuroscience, 3: 1027-1034 (2000)

Sharon, D. & Grinvald, A. Dynamics and constancy in cortical spatiotemporal patterns of orientation processing. *Science* **295**, 512–515 (2002).

Shoham, D. *et al.*Imaging cortical architecture and dynamics at high spatial and temporal resolution with new voltage- sensitive dyes. *Neuron***24**, 1–12 (1999).

Touryan, J., Felsen, G., and Dan, Y. Spatial structure of complex cell receptive fields measured with natural images. Neuron *45*, 781-791. (2005).

Touryan, J., Lau, B., and Dan, Y. Isolation of relevant visual features from random stimuli for cortical complex cells. J Neurosci *22*, 10811-10818. (2002).

Yao, H. and Dan, Y., Stimulus timing-dependent plasticity in cortical processing of orientation. *Neuron* **32**, pp. 315–323. (2001)

Yao, H., Shen, Y. and Dan, Y., Intracortical mechanism of stimulus-timing-dependent plasticity in visual cortical orientation tuning. *Proc. Natl. Acad. Sci. USA* **101**, pp. 5081–5086. (2004)

Chapter II. Excitatory and Suppressive Receptive Field Subunits in Awake Monkey V1

Overview

An essential step in understanding visual processing is to characterize the neuronal receptive fields (RFs) at each stage of the visual pathway, but RF characterization beyond V1 simple cells remains a major challenge. Recent application of spike-triggered covariance (STC) analysis has greatly facilitated characterization of complex cell RFs in anesthetized animals. Here we apply STC to RF characterization in awake monkey V1. We found up to 9 subunits for each cell, including one or two dominant excitatory subunits as described by the standard model, along with additional excitatory and suppressive subunits with weaker contributions. Compared to the dominant subunits, the non-dominant excitatory subunits prefer similar orientations and spatial frequencies but have larger spatial envelopes. They contribute to response invariance to stimulus orientation, position, and spatial frequency. In contrast, the suppressive subunits are tuned to orientations 45-90^{o} different from the excitatory subunits, which may underlie cross-orientation suppression. Together, the excitatory and suppressive subunits form a compact description of neuronal RFs in awake monkey V1, allowing prediction of the responses to arbitrary stimuli.

Introduction

The response properties of V1 neurons have been studied extensively over the past several decades. In the standard model, a simple cell RF consists of alternating ON and OFF subregions, which directly correspond to the orientation and spatial frequency tuning of the cell (Hubel and Wiesel, 1962; Movshon et al., 1978b). Complex cells exhibit orientation and spatial frequency tuning similar to simple cells, but they are insensitive to the contrast polarity and stimulus position within the RF. The energy model for complex cell RF consists of a pair of simple-cell-like subunits with the same orientation and spatial frequency tuning but different ON/OFF phases (Adelson and Bergen, 1985; Movshon et al., 1978a). This model accounts for the phase invariance as well as stimulus selectivity of complex cells.

To validate such RF models and to predict the responses of a given neuron to arbitrary visual stimuli, it is necessary to measure the RF structure quantitatively. For simple cells, spike-triggered average (STA) has been used effectively to estimate their RFs from the responses to sparse noise (Jones and Palmer, 1987) or white noise (Reid et al., 1997). For complex cells, however, since the outputs of different RF subunits are combined nonlinearly, these subunits cannot be estimated by STA. In previous studies, complex cell RFs have been studied by measuring the nonlinear interaction between paired stimuli (Emerson et al., 1987; Livingstone and Conway, 2003; Movshon et al., 1978a). Another method that has been used in recent studies is spike-triggered covariance (STC) analysis (Brenner et al., 2000; De Ruyter Van Steveninck and Bialek, 1988). Instead of averaging all the stimuli preceding spikes (as in STA), in STC analysis one

computes the covariance matrix of the spike-triggered stimulus ensemble and identifies the eigenvectors with eigenvalues significantly different from those of the entire stimulus ensemble. This method can reveal stimulus features that drive the neuron in a contrast-dependent but polarity invariant manner, and it has proved highly effective in the analysis of complex cell RF subunits in both cat (Felsen et al., 2005; Touryan et al., 2005; Touryan et al., 2002) and monkey (Rust et al., 2005) V1.

While the above studies have characterized the spatiotemporal structure of complex cell RFs in anesthetized animals, an ultimate challenge is to understand RF properties in the awake brain. Neuronal RFs in awake monkey V1 have been studied in phase-separated Fourier space (David et al., 2004). In the current study, we used STC to analyze the spatial structure of V1 RFs in awake, fixating monkeys. In addition to a dominant subunits that are consistent with the standard models for simple (Hubel and Wiesel, 1962; Movshon et al., 1978b) and complex (Adelson and Bergen, 1985; Movshon et al., 1978a) cells, we found additional excitatory subunits that contribute to orientation, position, and spatial frequency invariance. For some of the cells, we also found suppressive subunits (Rust et al., 2005), which are tuned to orientations up to 90^{o} different from the excitatory subunits. These subunits may contribute to cross-orientation suppression of V1 responses (Bonds, 1989). Including the non-dominant excitatory and suppressive subunits in the model significantly improved the prediction of neuronal responses to arbitrary white noise stimuli.

Methods

Electrophysiology recording

Single-unit recordings were made from V1 of three adult macaques (*Macaca mulatta*, two male, one female) using custom-made glass-coated tungsten electrodes (Li et al., 1995). Unit isolation was based on cluster analysis of waveforms and the presence of a refractory period determined from the autocorrelograms. Each recording epoch lasted for 5 min. All well isolated single units that lasted for ≥ 3 epochs were included in the analyses (maximum 25 epochs, n = 227). The RFs of these cells were 2-9^{o} from the fixation point (fovea). During each recording epoch, the monkey performed a continuous fixation task for juice reward. Eye position was monitored with a remote, infrared eye tracker (EYELINK II, resolution 0.01^{o} visual angle, sampling rate 500 Hz). An elliptical window was set for the eye position, whose vertical and horizontal axes were selected such that the kurtosis of data points within the window was 3 (mean vertical axis, 1.2^{o}; horizontal axis, 0.5^{o}). Data recorded during periods when the eye position was outside of this window were discarded (Figure 2.1.). In practice, however, the results were remarkably insensitive to the fixation window size. Similar results were obtained even when the window was set to infinity, perhaps because very few spikes were fired when the eye position was outside of the window and the stimuli fell outside of the RF. Surgery was conducted under aseptic conditions under deep pentobarbital anesthesia. All experimental procedures were performed in accordance with the National Institutes of Health guidelines.

Visual stimulation

Visual stimuli were generated with a PC and presented with a Sony Multiscan G520 monitor (size 30 × 40 cm, refresh rate 100 Hz, maximum luminance 80 cd m^{-2}). Luminance nonlinearities were corrected through software. Binary white noise stimuli (10 × 10 - 12 × 12 pixels, 100% contrast) were presented in an area slightly larger than the RF of the cell estimated by hand mapping. The stimuli were updated every 4 frames, resulting in an effective frame rate of 25 Hz. Each stimulus epoch consisted of 7500 frames (5 min), and the stimuli in different epochs were different. To test the prediction of the model based on the significant eigenvectors, a short white noise sequence (750 frames, 30 s) was repeated 4-70 times for each cell.

Spike-triggered covariance (STC) analysis

As described in previous studies (Rust et al., 2005; Touryan et al., 2005; Touryan et al., 2002), STC analysis identifies a set of visual features (represented by eigenvectors of the spike-triggered covariance matrix) that account for different amounts of variance (corresponding eigenvalues) in the spike-triggered stimulus ensemble. Thus it is well suited for identifying visual features that contribute to cortical responses in a contrast-dependent but polarity invariant manner.

The spike-triggered covariance matrix ($C_{m,n}$) was computed as:

$$C_{m,n} = \frac{1}{N}\sum_{i=1}^{N} S_m(i)S_n(i)$$

Where $S_m(i)$ and $S_n(i)$ are the luminance values of the mth and nth pixels in the stimulus preceding the ith spike, respectively, and N is the total number of spikes in the response. Eigenvalues and eigenvectors of this spike-triggered covariance matrix were computed.

To identify the significant eigenvectors, we first determined which eigenvectors of the spike-triggered stimulus ensemble had eigenvalues significantly different from the control eigenvalues (Figure 2.2A), defined as the eigenvalues of spike-triggered stimulus ensembles based on random spike trains (with the same number of spikes as the recorded spike train but random spike timing). The confidence intervals for the control eigenvalues were computed using 500 random spike trains (mean ± 4.4 SD, corresponding to a significance level of $p < 10^{-4}$). We then identified eigenvalues that stood out from the rest of the eigenvalues of the spike-triggered ensemble by calculating the difference between neighboring eigenvalues (Figure 2.2B). The confidence intervals were set at mean ± 4.4 SD of the difference values, computed after excluding the first and last five eigenvalues (which are likely to be significant eigenvalues with large differences from their neighbors). If a point is found beyond the confidence intervals for the difference criterion, all the eigenvalues preceding (for excitatory eigenvectors) or following (for suppressive eigenvectors) this point are considered significant by this criterion. Eigenvalues that satisfy both criteria are considered significant. Note that although in principle only the first criterion (Figure 2A) is necessary for eigenvector identification (Rust et al., 2005; Touryan et al., 2002), in practice we found that incorporating the second criterion (Figure 2B) significantly reduced false positives (Touryan et al., 2005).

In most of the analyses (Figures 2.2-6) we focused on the spatial structure of the RF by performing STC at the optimal frame (either 1 or 2 frames before each spike) in order to improve the signal-to-noise ratio of the estimate. For predicting the responses to white noise stimuli (Figure 2.7), however, both frames were included to estimate the spatiotemporal RF subunits.

Note that to compute the standard covariance matrix, the average of the spike-triggered ensemble (STA) should be subtracted from each stimulus. In some implementations of STC, STA is first weighted before subtracted from each stimulus to ensure that the eigenvectors of STC are all orthogonal to STA (Rust et al., 2005). We believe that the treatment of STA is largely a matter of individual preference, as long as the specific choice is taken into consideration when interpreting the result of STC. As in our previous implementations of STC (Touryan et al., 2005; Touryan et al., 2002), STA was not subtracted in the current study. As a result, the first eigenvector (with the largest eigenvalue) of simple-cell-like neurons is often similar to STA.

As pointed out in previous studies (Paninski, 2003; Rust et al., 2005), the use of binary white noise may result in artifacts in the identification of suppressive eigenvectors, due to tapering of the stimulus distribution (reduction of variance) as one moves away from the origin along particular directions. The resulting spurious suppressive eigenvectors are related to the excitatory eigenvectors (which happen to lie close to these particular directions) rather than reflecting the suppressive features of the neuron. To reduce such artifacts, we used the method described by Rust et al. (2005). Briefly, we computed the pooled response of the significant excitatory eigenvectors to each stimulus based on their relative weights (see below), divided these stimuli into 10 equal-sized subsets according to their pooled responses, and then whitened each subset by multiplying by

$$E_e E_e^T + E_o E_n D_n^{-1/2} E_n^T E_o^T$$

where the matrix E_e contains the significant excitatory eigenvectors, E_o contains all the other eigenvectors, and E_n and D_n are eigenvectors and eigenvalues of the covariance matrix of the *n*th subset. The whitened stimuli were then used to estimate the significant suppressive eigenvectors.

Relative weights of subunits

The contribution of each significant eigenvector (V) to the neuronal response depends not only on the contrast of the eigenvector in the particular stimulus S_i (vector contrast is computed as $S_i \bullet V$), but also on the gain of the contrast-response function for this eigenvector. This gain was estimated by fitting the contrast-response function for each eigenvector by $r = a(S \bullet V)^2 + b$, where r is the firing rate as a function of vector contrast (computed from the same data used for STC analysis), and a and b are free parameters (Touryan et al., 2005; Touryan et al., 2002). The relative weight of each significant eigenvector is defined as $\sqrt{|a|}$, which is used for computing the pooled spatial envelope and Fourier spectrum (Figure 2.4) and the pooled responses for predicting the orientation tuning (Figures 2.6) and the responses to white noise (Figure 2.7).

Prediction of responses to arbitrary stimuli

To predict the response of each cell to arbitrary visual stimuli, we fitted the following function to the recorded responses:

$$r = \alpha + (\beta E - \delta S)/(\gamma E + \varepsilon S + 1)$$

where E is the pooled response of the excitatory eigenvectors, S is the pooled response of the suppressive eigenvectors (computed with the relative weight of each eigenvector, see

above), and α, β, δ, γ, and ε are free parameters. This is similar to the model used by Rust et al. (2005), which allows both subtractive and divisive contributions of the suppressive eigenvectors. Values for the free parameters were fit to minimize the mean-squared error for the "training data", which are the responses to white noise stimuli used to estimate the significant eigenvectors.

Results

We made single-unit recordings from 227 V1 neurons in three macaque monkeys performing a fixation task. Visual stimuli were binary white noise ($10 \times 10 - 12 \times 12$ pixels, 25 frames/s) presented in an area slightly larger than the classical RF of the cell. During presentation of each stimulus sequence (7500 frames, 5 min), the eye position was monitored continuously. Recordings from the periods in which the eye position was outside of a fixation window were excluded from analyses (Figure 2.1.A).

The stimulus preceding each spike was collected to form the spike-triggered stimulus ensemble (Figure 2.1.B), and the covariance matrix of this ensemble was computed. Significant eigenvalues were identified as those that were significantly different from (1) the control eigenvalues calculated based on randomized spike trains (Figure 2.2A) and (2) their neighboring eigenvalues (Figure 2.2B) (Experimental Procedures). For 145 of the 227 cells studied, we found at least one significant eigenvalue. The eigenvectors with significantly higher eigenvalues represent stimulus features that excite the cell (Touryan et al., 2005; Touryan et al., 2002), whereas those with significantly lower eigenvalues reflect suppressive features that reduce neuronal firing (Rust et al., 2005).

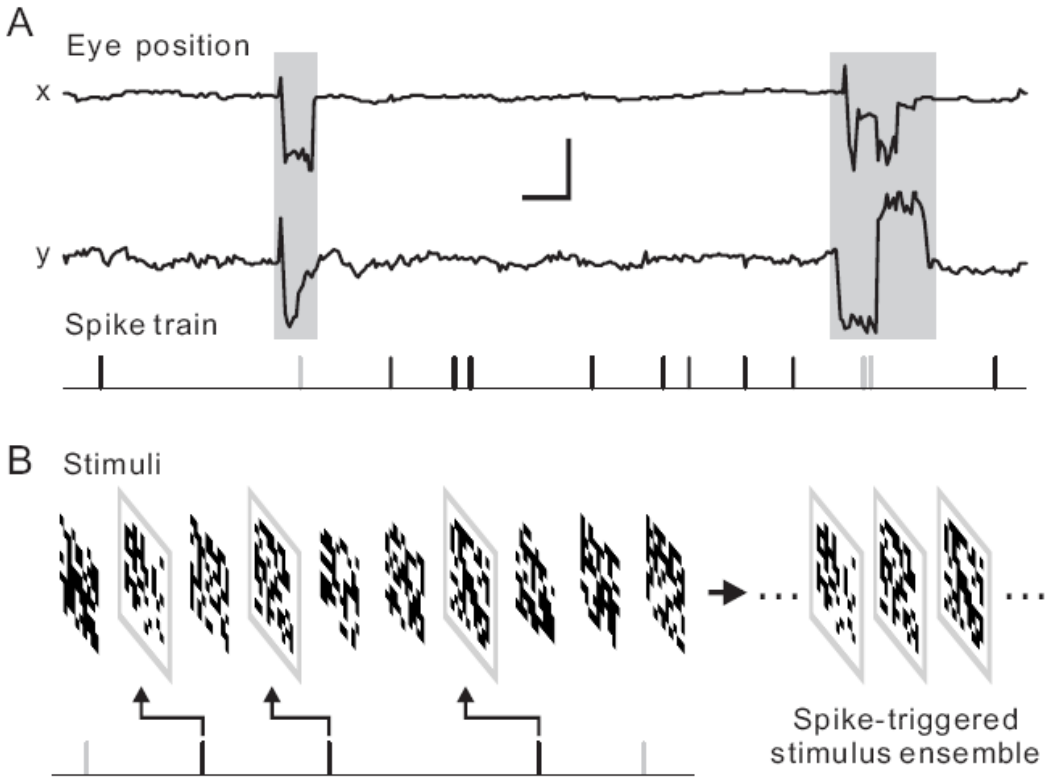

Figure 2.1. Illustration of experimental and analysis procedures

(A) Example eye position traces (x, horizontal; y, vertical) recorded by an infrared eye tracker (sampled at 500 Hz) during a recording epoch. Gray shading indicates periods when eye position was outside of fixation window. Corresponding segments of the spike train (bottom) were excluded from analysis. Gray, excluded spikes. Scale bars: 1s, 1^{o}.

(B) White noise stimuli. Gray box indicates stimulus frame preceding each spike.

Structure of excitatory and suppressive eigenvectors

The significant eigenvectors of each cell can be divided into three groups, based on their spatial structure and their corresponding eigenvalues. The first group consists of one or a pair of eigenvectors, whose eigenvalues stood out most prominently above the rest. These excitatory eigenvectors, referred to as the “dominant eigenvectors”, were

almost always Gabor-like. Most of the complex cell-like neurons, whose responses to drifting gratings were only weakly modulated at the temporal frequency of the grating (Skottun et al., 1991), contained a pair of dominant eigenvectors (e.g., both example cells in Figure 2.2). These eigenvectors were similar to each other in size, orientation, and spatial frequency, but different in phase (Figure 2.2C), consistent with the pair of subunits in the energy model for complex cell RF (Adelson and Bergen, 1985; Movshon et al., 1978a). On the other hand, cells with strong temporal modulations (simple cell-like) are likely to have a single dominant eigenvector (i.e., the largest jump is between the first and the second eigenvalues). This eigenvector typically resembled STA (data not shown), which represents the linear RF of the simple cell. Note that we did not strictly distinguish between simple and complex cells here because recent studies suggested that V1 neurons fall on a simple/complex continuum rather than two distinct classes (Chance et al., 1999; Mechler and Ringach, 2002).

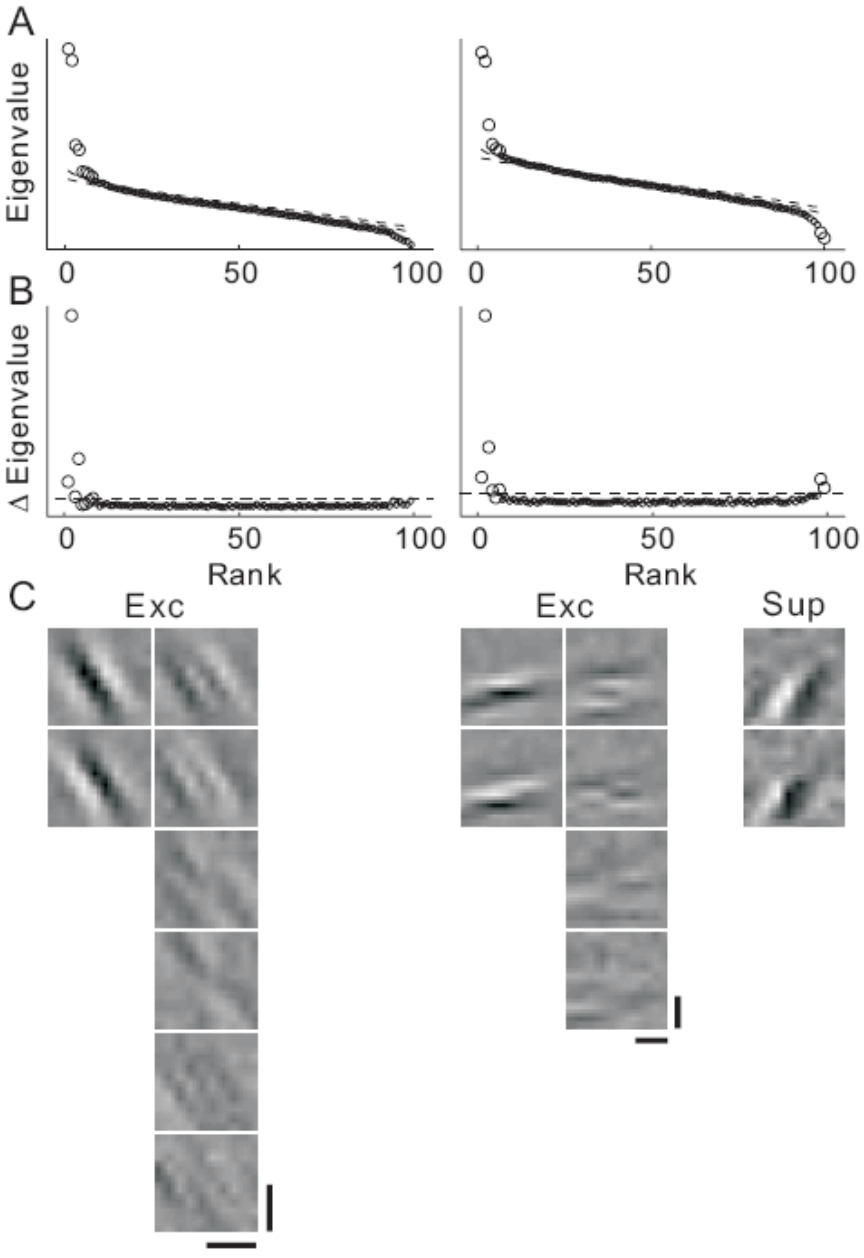

Figure 2.2. Identification of significant eigenvectors, illustrated with two example cells (left and right columns) (A) Eigenvalues of spike-triggered covariance matrix. Dashed lines, control confidence intervals ($p < 10^{-4}$).

(B) Difference between neighboring eigenvalues. Dashed line, confidence interval for the difference ($p < 10^{-4}$). Large circles, significant eigenvalues satisfying both criteria in (A) and (B).

(C) Significant eigenvectors. The contrast of each eigenvector is scaled by its relative weight (see Experimental Procedures). Excitatory and suppressive eigenvectors are scaled separately. Scale bars: 0.5°.

Many simple- or complex-like neurons also exhibited additional excitatory eigenvectors (Figure 2.3B), whose eigenvalues showed smaller but significant upward jumps (Figures 2.2A & 2.2B). This second group of eigenvectors, referred to as the "non-dominant" excitatory eigenvectors, were oriented similarly to the dominant eigenvectors but showed more complex spatial structures and larger sizes (Figures 2.2C and 2.3A). For 38 cells, we also found the third group of eigenvectors with significantly lower eigenvalues. Most of these suppressive eigenvectors (Figure 2.2, second cell; Figure 2.3A, third and fourth cells) are oriented quite differently from the excitatory eigenvectors. It is important to note that although these significant eigenvectors provide a functional representation of the RF structure that is indicative of the response properties of the presynaptic neurons, each significant eigenvector does not necessarily represent the RF of an individual presynaptic cell (i.e., an "anatomical subunit"). Instead, it is likely to represent a linear combination of multiple anatomical subunits (Rust et al., 2005; Touryan et al., 2002). However, as a convenient functional description, we refer to these significant eigenvectors as the excitatory or suppressive RF subunits.

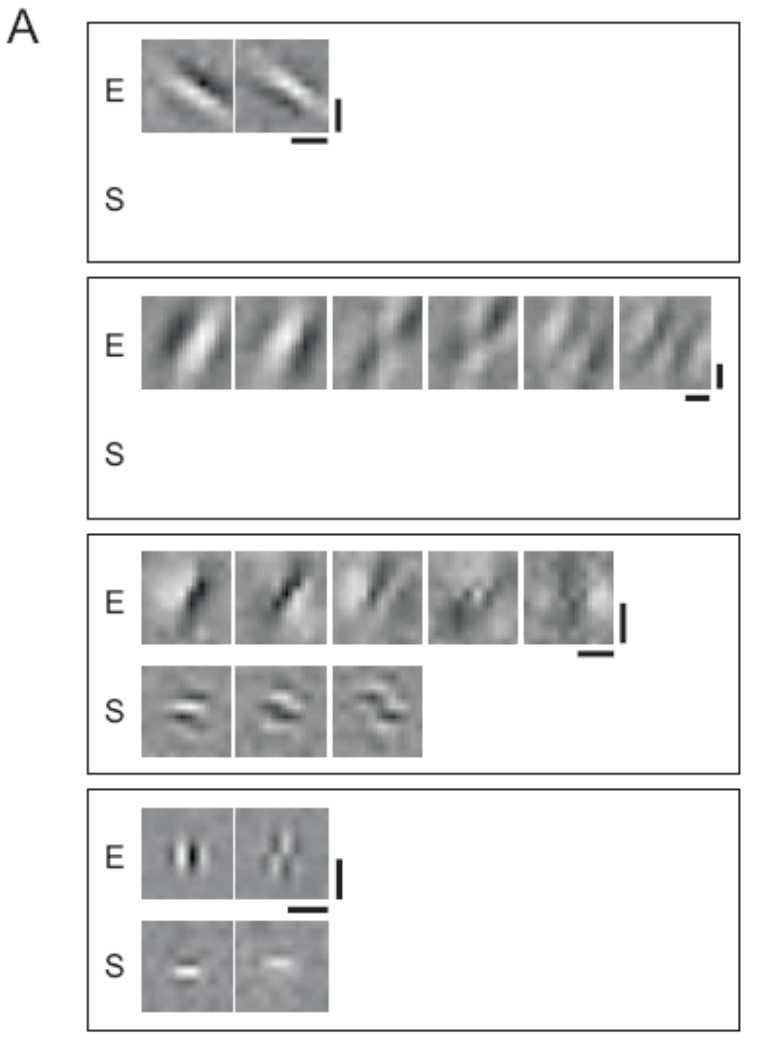
A
E
S
E
S
E
S
E
S
B
# of cells
30
20
10
0
# of eigenvectors (sup)
0
1
2
3
4
# of eigenvectors (exc)
0
1
2
3
4
5
6
7
8

Figure 2.3. Number of significant eigenvectors for each cell

(A) Significant eigenvectors for four example cells. E, excitatory, S, suppressive. Scale bars: 0.5°.

(B) Summary of number of excitatory and suppressive eigenvectors per cell. Cells with no significant eigenvector were not included.

Relationship between different subunit groups

To understand the relationship between the three groups of subunits of each cell, we first compared their locations and sizes by computing the pooled spatial envelope of each group (square root of the weighted sum of squares of all the subunits in each group, see Experimental Procedures) (Rust et al., 2005). Compared to the dominant group, the non-dominant excitatory subunits showed a larger spatial envelope (Figure 2.4A, 2.4C). This is similar to the finding in anesthetized monkey V1 (Rust et al., 2005), which could be explained if the non-dominant eigenvectors represent linear combinations of multiple anatomical subunits that are spatially displaced from each other. The suppressive subunits, on the other hand, largely overlapped with the dominant subunits in space. Quantitative comparison of the subunit sizes for the population of cells is summarized in Figure 2.5A and 2.5B, based on the width-at-half-height of each pooled envelope along the preferred orientation of the dominant subunits (length) and along the perpendicular axis (width).

We also compared the spatial frequency and orientation tuning of the three groups of subunits based on the pooled spatial spectrum of each group (Figure 2.4B). The spectrum of the non-dominant excitatory group largely overlapped with that of the dominant group, indicating similar orientation and spatial frequency tuning (Figure 2.4C). In contrast, the spectrum of the suppressive subunits showed little overlap with those of

the excitatory groups. As shown in Figure 2.4B and 2.4C, the separation between the excitatory and suppressive subunits in spatial spectrum was more pronounced along the angular than the radial axis, indicating major differences in orientation as opposed to spatial frequency tuning. For the population of cells, the preferred spatial frequency and orientation of the non-dominant excitatory subunits were closely correlated with those of the dominant subunits (Figure 2.5C and 2.5D, upper panel), but the suppressive subunits showed larger deviations in spatial frequency tuning and up to 90^{o} difference in preferred orientation (lower panel).

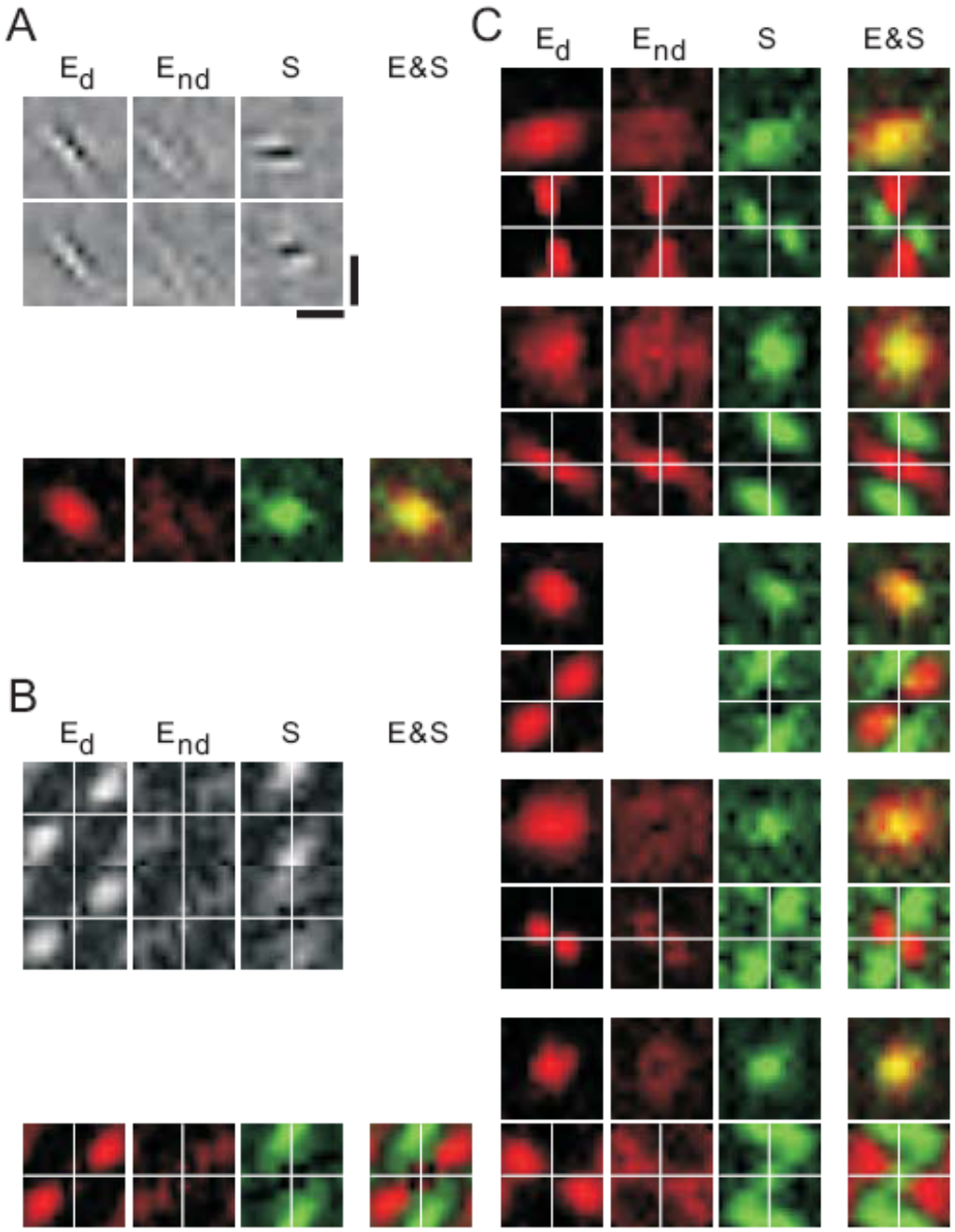

Figure 2.4. Spatial and spectral relationships among different subunit groups

(A) Top panel: Dominant and non-dominant excitatory (E_d and E_{nd}) and suppressive (S) subunits of an example cell. Scale bars: 0.5^o. Bottom panel: pooled spatial envelope of each group of subunits. Red, excitatory; green, suppressive. The envelopes of all three

groups are superimposed on the right; yellow indicates overlap between excitatory and suppressive envelopes.

(B) Top panel: Spatial frequency spectrum of each subunit shown in (A). Bottom panel: Pooled frequency spectrum of each group.

(C) Pooled spatial envelopes (upper row) and frequency spectra (lower row) of the three groups of subunits for five example cells.

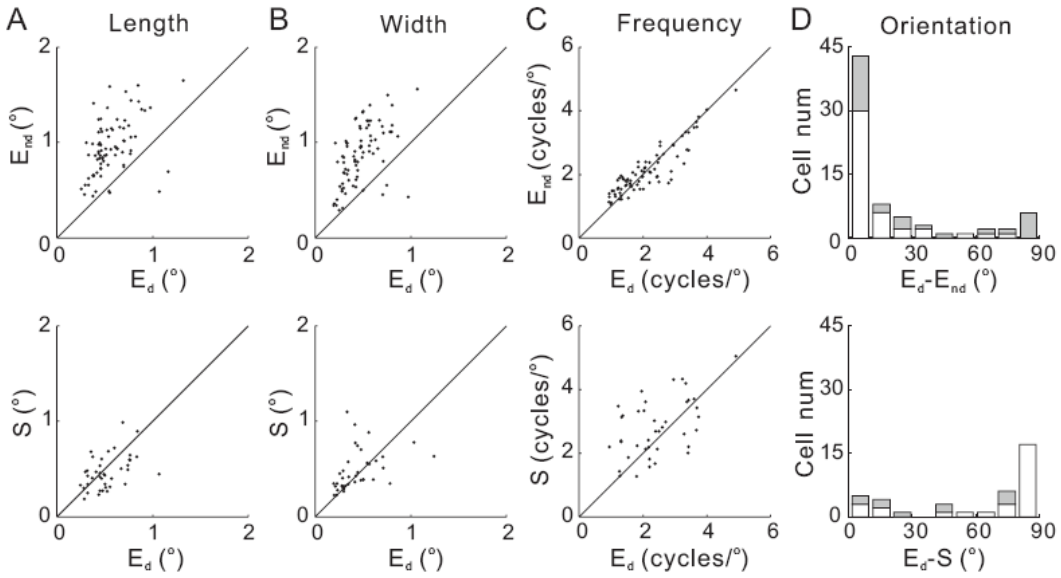

Figure 2.5. Quantitative comparison of non-dominant excitatory subunits (E_{nd}) and suppressive (S) subunits to the dominant (E_d) subunits

(A, B) Length and width of pooled spatial envelope, measured by width at half height. Each point represents one cell (n = 79). There are fewer data points in the lower plots because fewer cells have suppressive subunits.

(C) Optimal spatial frequency measured by peak position of the frequency spectrum, for the same populations of cells shown in (A) and (B).

(D) Distribution of difference in preferred orientation. White bars, cells with clear tuning (circular variance of tuning curve < 0.7); gray bars, poorly tuned cells (circular variance

> 0.7). Circular variance is defined as $1-\left|\sum_k R_k e^{i2\theta_k}\right| / \sum_k R_k$, where R_k is the response at orientation θ_k, $0 < \theta_k < 180^o$.

Response Invariance

The angular separation between the excitatory and suppressive subunits in the spectral domain suggests that the suppressive subunits contribute to cross-orientation suppression (Bonds, 1989), which should enhance the selectivity of V1 neurons. What is the function of the non-dominant excitatory subunits? Since each excitatory eigenvector is likely to represent a linear combination of multiple anatomical subunits (Rust et al., 2005; Touryan et al., 2002), and conversely an anatomical subunit may be described as a combination of eigenvectors, we examined various linear combinations of the excitatory eigenvectors. The neuronal responses to combinations of eigenvectors can be characterized by joint contrast-response functions (Rust et al., 2005; Touryan et al., 2002).

Figure 6A shows the joint contrast-response functions for four pair-wise combinations of the excitatory subunits of an example cell. The contrast of a given subunit in each stimulus is defined as the dot product of the eigenvector and the stimulus, and the neuronal firing rate is plotted against the contrasts of each pair of subunits. Consistent with previous findings in cat V1 (Touryan et al., 2002), each linear combination of the dominant pair of subunits is also Gabor-like (Figure 2.6A, top left), with the spatial phase of the Gabor function shifting with the relative weights of the two subunits (angular coordinate of the 2-D function). The circularly symmetric joint contrast-response function is thus consistent with the known phase invariance of complex

cells (Adelson and Bergen, 1985; Hubel and Wiesel, 1962; Movshon et al., 1978a). Interestingly, linear combinations between a dominant and a non-dominant excitatory subunit revealed other forms of invariance. For this example cell, although the third (non-dominant) eigenvector contained fractured ON and OFF subregions, its combinations with the first (dominant) eigenvector resulted in Gabor-like patterns at different orientations (upper right plot, compare patterns in the three boxes). Furthermore, combinations between the second and the third eigenvectors resulted in Gabor patterns at different positions (lower left plot), and those between the second and fifth exhibited different spatial frequencies (lower right plot). Since the non-dominant subunits make weaker contributions to the response than the dominant subunits, the joint contrast-response functions did not exhibit perfect circular symmetry. Nevertheless, the existence of these weaker excitatory subunits enhances the response invariance with respect to small changes in stimulus orientation, position, and frequency (Berkes and Wiskott, 2006). A plausible anatomical basis for the observed invariance is that the neuron receives inputs from a set of presynaptic neurons with slightly different preferred orientations, RF positions, and spatial frequencies.

The above three types of invariance were also observed in other cells, with orientation invariance the most common among our samples. We thus further quantified the effect of non-dominant excitatory subunits on orientation tuning. The tuning of each subunit was computed as its responses to sinusoidal gratings at a range of orientations at the optimal spatial frequency for the dominant subunits. Since previous studies have shown that the excitatory subunits contribute additively to the neuronal responses (Rust et al., 2005; Touryan et al., 2002), the tuning of the cell was predicted as the weighted sum

of the tuning of all excitatory subunits, with the weight of each subunit proportional to its contrast-response gain (see Experimental Procedures). As shown in Figure 2.6B, including the non-dominant excitatory subunits in the prediction significantly broadened the tuning for this example cell. For the population of cells with well-tuned excitatory eigenvectors, including the non-dominant excitatory subunits significantly increased the width of the tuning curve (Figure 2.6C, $p < 0.01$, Wilcoxon signed rank test). Notably, the effects of the non-dominant excitatory subunits and the suppressive subunits on orientation tuning do not simply cancel each other. While the non-dominant excitatory subunits render the neuron less sensitive to small variations around the optimal orientation, the suppressive subunits reduce the responses near the orthogonal orientation without necessarily narrowing the tuning curve (Figure 2.6B, inset).

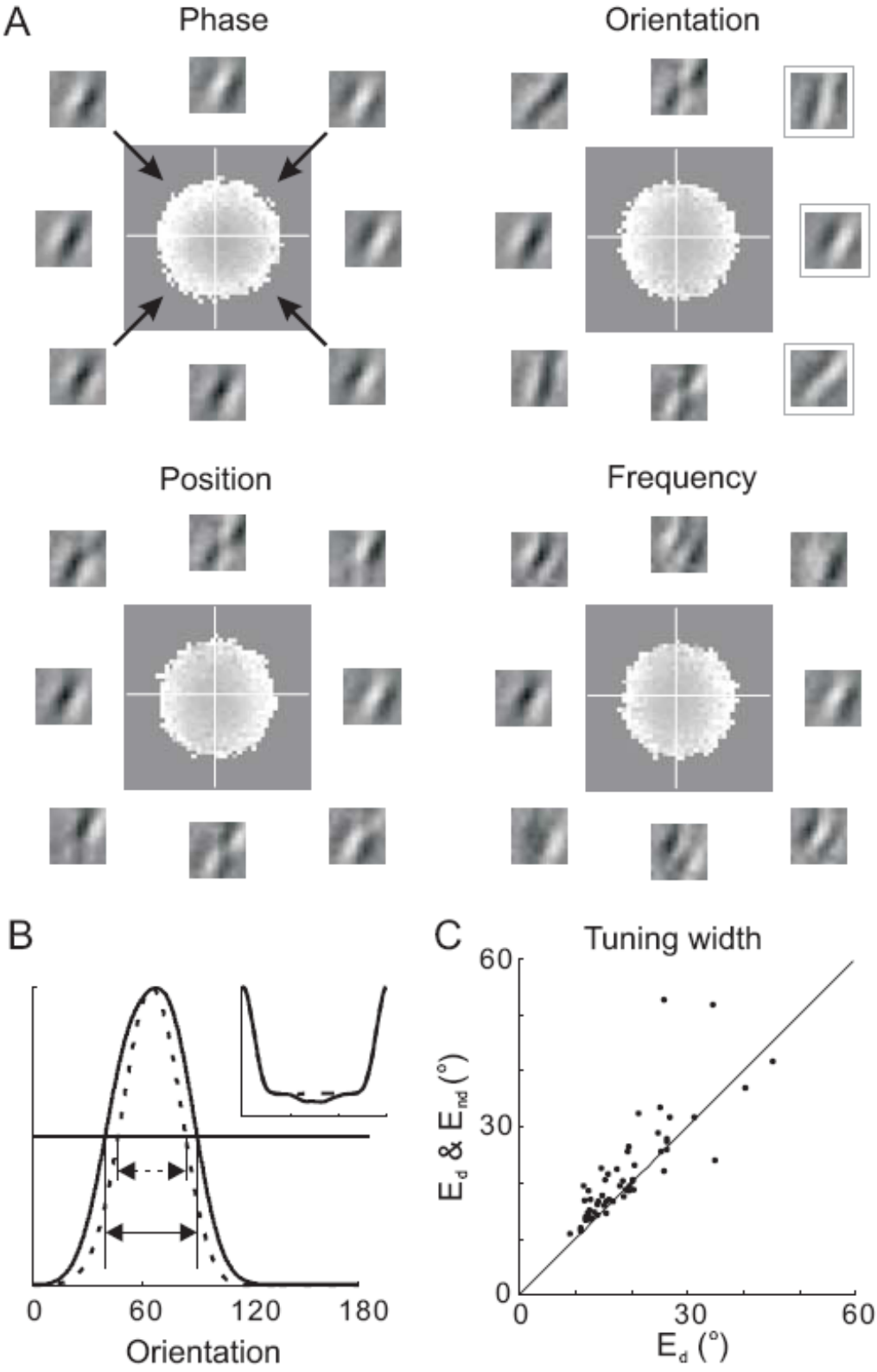
A
Phase
Orientation
Position
Frequency
B
0
60
120
180
Orientation
C
Tuning width
60
30
0
E_d & E_{nd} (°)
0
30
60
E_d (°)

Figure 2.6. Phase, orientation, position, and frequency invariance

(A) Joint contrast-response functions of a complex cell (second cell in Figure 3A) with six excitatory subunits, for different pair-wise combinations of the excitatory subunits. Large square in the middle: firing rate (luminance coded) plotted against the contrasts of the pair of subunits. Small outer plots: stimulus patterns corresponding to selected points (arrows) in the joint contrast-response functions.

(B) Orientation tuning of the cell predicted based on the dominant pair alone (dashed) and based on all excitatory subunits (solid). Arrows indicate width at half height of the tuning curves. Inset, predicted tuning curves of another example cell, based on only the excitatory subunits (dashed) and based on both excitatory and suppressive subunits (the contribution of suppressive subunits was modeled subtractively for qualitative illustration).

(C) Predicted tuning width based on all excitatory eigenvectors vs. that based on the dominant subunits alone. Each point represents one cell; only cells with clear tuning (circular variance < 0.6) were included (n = 56).

Predictions of responses to white noise

Finally, to assess the RF model based on the excitatory and suppressive subunits, we predicted the response of each cell to a short white-noise test sequence (30 sec, repeated 4-70 times) using (I) dominant subunits alone, (II) all excitatory subunits, and (III) all excitatory and suppressive subunits. Following the implementation of Rust et al. (2005), the responses of the excitatory subunits and those of the suppressive subunits were first summed separately using weights proportional to their contrast-response gains. The excitatory and suppressive components were then combined with a nonlinear function that allows both subtractive and divisive interactions (Experimental Procedures). Figure 2.7A shows the measured response of an example cell (gray shading) and the

predictions based on the dominant subunits alone (black line, model I) and based on all excitatory and suppressive subunits (red line, model III). Although the model based on the dominant subunits alone predicted the main temporal variations of the measured response, including the non-dominant excitatory and suppressive subunits improved the prediction by alleviating both under- and over-estimation of the peak amplitudes (Figure 7A, arrow heads).

We measured the quality of prediction by each model using correlation coefficient between the predicted and measured responses for the population of cells. Compared to the model based on the dominant subunits alone, including the non-dominant excitatory subunits significantly improved the prediction for the population of cells (Figure 2.7B, $p < 0.01$, Wilcoxon signed rank test, $n = 83$). Including the suppressive subunits led to a small further improvement, although the effect was not significant (Figure 2.7C, $p = 0.09$, $n = 31$). Even with the full model, however, the correlation coefficient between the predicted and measured responses was lower than that between measured responses averaged from different repeats (Figure 2.7D), indicating that the prediction error could not be accounted for by noise in the measured responses. The incompleteness of the model may be due to additional subunits not identified by the STC analysis or to noise in the estimated subunit RFs, both of which depend on the amount of data (Aguera y Arcas and Fairhall, 2003; Paninski, 2003) that is limited from recordings in awake monkeys. More importantly, the responses are likely to exhibit other forms of nonlinearity such as contrast adaptation (Maffei et al., 1973), which are not captured by the subunit RF model used in this study.

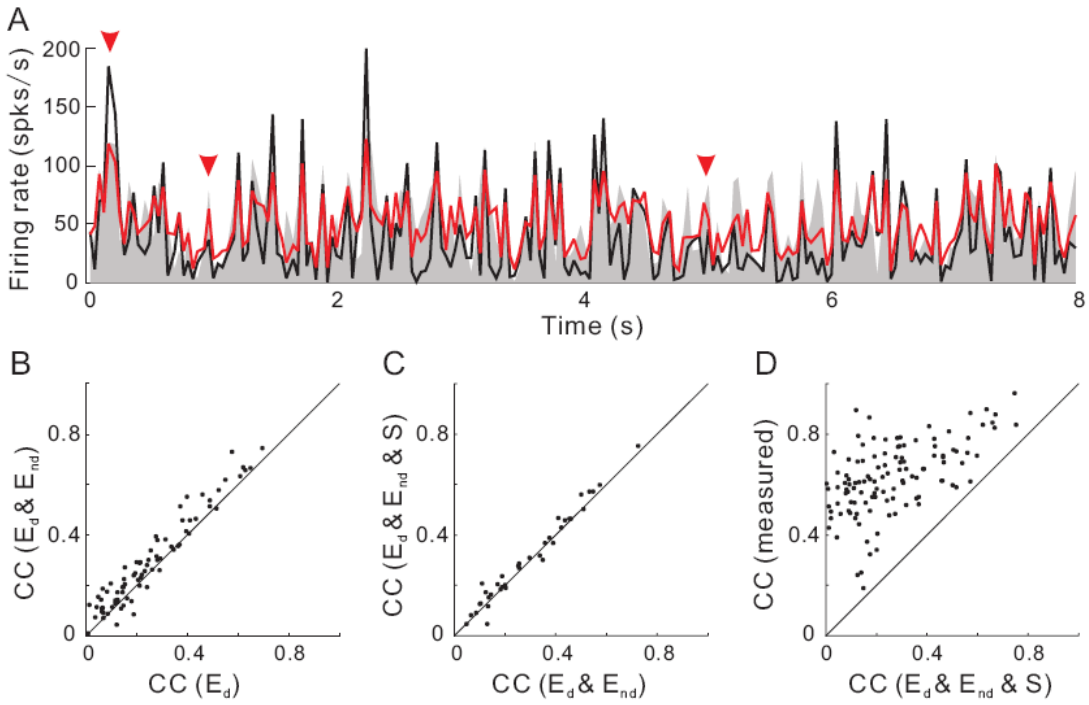

Figure 2.7. Prediction of responses to arbitrary white noise stimuli

(A) Comparison of predicted and measured firing rates of an example cell. Gray shading: measured response, averaged from 24 repeats of the test stimulus. Black line: Prediction based on the dominant pair of subunits. Red line: Prediction based on all subunits (6 excitatory and 1 suppressive). Red arrow heads, firing rate peaks better predicted by the model including all subunits.

(B) Improvement of prediction by non-dominant excitatory subunits. Correlation coefficient (CC) between the measured and predicted responses based on all excitatory subunits vs. CC with only the dominant subunits. Each symbol represents one cell (n = 83).

(C) Improvement of prediction by suppressive subunits. CC based on both excitatory and suppressive subunits vs. CC based on only the excitatory subunits (n = 39).

(D) CC between measured responses (averaged from two non-overlapping sets of repeats) vs. CC between predicted (based on all excitatory and suppressive subunits) and measured responses (n = 123).

Discussion

The current study together with several other STC analyses (Felsen et al., 2005; Rust et al., 2005; Touryan et al., 2005; Touryan et al., 2002) suggest the following model for V1 classical RFs. The dominant RF component is a Gabor-like subunit for simple cells and a pair of subunits for complex cells. This component is consistent with the standard existing model (Adelson and Bergen, 1985; Hubel and Wiesel, 1962; Movshon et al., 1978a; Movshon et al., 1978b). In both anesthetized and awake monkeys, however, STC analysis has allowed identification of two additional groups of subunits: the non-dominant excitatory and suppressive subunits, whose contributions to cortical responses are weaker than the dominant component, at least under white noise stimulation. The non-dominant excitatory subunits are more dispersed spatially but overlap substantially with the dominant component in the frequency spectrum (Figures 2.4, 2.5), and they contribute to response invariance with respect to small changes in stimulus orientation, position, and frequency (Figure 2.6). In contrast, the suppressive subunits overlap with the dominant component spatially but are complementary in the frequency spectrum. They are likely to mediate suppression of the responses to “antagonistic” visual features, including those at the orthogonal orientation (Figures 2.4, 2.5) or opposite motion direction (Rust et al., 2005). Invariance and selectivity of neuronal responses are both important for visual processing. As shown in Figure 2.7, incorporating the non-dominant excitatory and suppressive subunits in the model improves the prediction of cortical responses to arbitrary white noise stimuli.

In previous studies in anesthetized cat V1 (Felsen et al., 2005; Touryan et al., 2005; Touryan et al., 2002), we found that most complex cell RFs consist of a pair of Gabor-like subunits, and non-dominant excitatory or suppressive subunits were rarely observed. This may be due to differences in the number of spikes used in the STC analysis, in the signal/noise ratio of the cortical responses, or in the number or strength of the non-dominant subunits. Regardless of the underlying reason, the fact that the non-dominant excitatory and suppressive subunits are readily observed in V1 of both anesthetized (Rust et al., 2005) and awake monkeys suggests that there are substantial inter-species differences in the number of RF subunits identifiable by the STC analysis.

Although there are important similarities between our findings and those of Rust et al. (2005) in the types of RF subunits and their spatial and spectral relationships, there is a noticeable difference in the relative contribution of the non-dominant subunits. While Rust et al. found that including the non-dominant subunits dramatically improved the prediction of cortical responses, in our case the improvement measured by correlation coefficient between the predicted and measured responses was relatively small (Figure 2.7). This discrepancy may be largely due to the difference in the visual stimuli used for testing the models. While we used arbitrary white noise stimuli, the test stimuli used by Rust et al. were matched to the non-dominant subunits in spatiotemporal patterns and are thus likely to emphasize their contributions to the responses.

Our results have shown that STC analysis is highly effective for characterizing the neuronal RF subunits in awake monkey V1. While the current study is performed with white noise stimuli during a simple fixation task, future studies using similar analysis techniques will allow us to examine the RF properties under more naturalistic visual

stimulation (David et al., 2004; Touryan et al., 2005) and behavioral conditions. These studies may reveal novel RF properties related to natural scene statistics (Felsen et al., 2005; Sharpee et al., 2006) and task-dependent top-down modulation of cortical processing (Fritz et al., 2003; Li et al., 2004).

References

Adelson, E. H., and Bergen, J. R. (1985). Spatiotemporal energy models for the perception of motion. J Opt Soc Am A *2*, 284-299.

Aguera y Arcas, B., and Fairhall, A. L. (2003). What causes a neuron to spike? Neural Comput *15*, 1789-1807.

Berkes, P., and Wiskott, L. (2006). On the analysis and interpretation of inhomogeneous quadratic forms as receptive fields. Neural Comput *18*, 1868-1895.

Bonds, A. B. (1989). Role of inhibition in the specification of orientation selectivity of cells in the cat striate cortex. Vis Neurosci *2*, 41-55.

Brenner, N., Bialek, W., and de Ruyter van Steveninck, R. (2000). Adaptive rescaling maximizes information transmission (see comments). Neuron *26*, 695-702.

Chance, F. S., Nelson, S. B., and Abbott, L. F. (1999). Complex cells as cortically amplified simple cells. Nat Neurosci *2*, 277-282.

David, S. V., Vinje, W. E., and Gallant, J. L. (2004). Natural stimulus statistics alter the receptive field structure of v1 neurons. J Neurosci *24*, 6991-7006.

De Ruyter Van Steveninck, R., and Bialek, W. (1988). Real-time performance of a movement-sensitive neuron in the blowfly visual system: Coding and information transfer in short spike sequences. Proceedings of the Royal Society of London Series B Biological Sciences *234*, 379-414.

Emerson, R. C., Citron, M. C., Vaughn, W. J., and Klein, S. A. (1987). Nonlinear directionally selective subunits in complex cells of cat striate cortex. J Neurophysiol *58*, 33-65.

Felsen, G., Touryan, J., Han, F., and Dan, Y. (2005). Cortical sensitivity to visual features in natural scenes. PLoS Biol *3*, e342.

Fritz, J., Shamma, S., Elhilali, M., and Klein, D. (2003). Rapid task-related plasticity of spectrotemporal receptive fields in primary auditory cortex. Nat Neurosci *6*, 1216-1223.

Hubel, D. H., and Wiesel, T. N. (1962). Receptive fields, binocular interaction and functional architecture in the cat's visual cortex. J Physiol (Lond) *160*, 106-154.

Jones, J. P., and Palmer, L. A. (1987). The two-dimensional spatial structure of simple receptive fields in cat striate cortex. J Neurophysiol *58*, 1187-1211.

Li, C. Y., Xu, X. Z., and Tigwell, D. (1995). A simple and comprehensive method for the construction, repair and recycling of single and double tungsten microelectrodes. J Neurosci Methods *57*, 217-220.

Li, W., Piech, V., and Gilbert, C. D. (2004). Perceptual learning and top-down influences in primary visual cortex. Nat Neurosci *7*, 651-657.

Livingstone, M. S., and Conway, B. R. (2003). Substructure of direction-selective receptive fields in macaque V1. J Neurophysiol *89*, 2743-2759.

Maffei, L., Fiorentini, A., and Bisti, S. (1973). Neural correlate of perceptual adaptation to gratings. Science *182*, 1036-1038.

Mechler, F., and Ringach, D. L. (2002). On the classification of simple and complex cells. Vision Res *42*, 1017-1033.

Movshon, J. A., Thompson, I. D., and Tolhurst, D. J. (1978a). Receptive field organization of complex cells in the cat's striate cortex. J Physiol (Lond) *283*, 79-99.

Movshon, J. A., Thompson, I. D., and Tolhurst, D. J. (1978b). Spatial summation in the receptive fields of simple cells in the cat's striate cortex. J Physiol *283*, 53-77.

Paninski, L. (2003). Convergence properties of three spike-triggered analysis techniques. Network *14*, 437-464.

Reid, R. C., Victor, J. D., and Shapley, R. M. (1997). The use of m-sequences in the analysis of visual neurons: linear receptive field properties. Vis Neurosci *14*, 1015-1027.

Rust, N. C., Schwartz, O., Movshon, J. A., and Simoncelli, E. P. (2005). Spatiotemporal elements of macaque v1 receptive fields. Neuron *46*, 945-956.

Sharpee, T. O., Sugihara, H., Kurgansky, A. V., Rebrik, S. P., Stryker, M. P., and Miller, K. D. (2006). Adaptive filtering enhances information transmission in visual cortex. Nature *439*, 936-942.

Skottun, B. C., De Valois, R. L., Grosof, D. H., Movshon, J. A., Albrecht, D. G., and Bonds, A. B. (1991). Classifying simple and complex cells on the basis of response modulation. Vision Res *31*, 1079-1086.

Touryan, J., Felsen, G., and Dan, Y. (2005). Spatial structure of complex cell receptive fields measured with natural images. Neuron *45*, 781-791.

Touryan, J., Lau, B., and Dan, Y. (2002). Isolation of relevant visual features from random stimuli for cortical complex cells. J Neurosci *22*, 10811-10818.

Chapter III. Rapid Learning in Visual Cortical Coding of Natural Scenes

Overview

Experience-dependent plasticity in adult visual cortex is believed to play important roles in visual coding and perceptual learning. Here we show that repeated stimulation with movies of natural scenes induces a rapid improvement of response reliability in cat visual cortex, an effect largely absent with white noise and flashed bar stimuli. The improved reliability can be accounted for by a selective increase in spiking evoked by preferred stimuli, and the magnitude of improvement depends on the sparseness of the response. The increase in reliability persists for at least several minutes in the absence of further movie stimulation. During this period, there is detectable reverberation of the movie-evoked responses in the spontaneous spiking activity. Thus, repeated exposure to natural stimuli not only induces a rapid improvement of cortical response reliability, but also leaves a "memory trace" in subsequent spontaneous activity.

Introduction

Visual stimulation can modify cortical circuitry and response properties on multiple time scales. For example, in contrast adaptation, exposure to high-contrast stimuli for seconds to minutes causes a reduction in response amplitude (Maffei, 1973 #30) and changes in stimulus selectivity (Movshon, 1979 #31) (Dragoi, 2000 #33; Muller, 1999 #32) of cortical neurons. These changes may be due to reduced neuronal excitability (Carandini, 1997 #36; Sanchez-Vives, 2000 #35) or short-term synaptic depression (Chance, 1998 #45). On the time scale of several minutes, synchronous visual stimulation within the receptive field and in a non-responsive surround region causes an expansion of the receptive field into the co-stimulated surround (Eysel, 1998 #34), which could be accounted for by Hebbian synaptic plasticity (Hebb, 1949 #26). Recent studies have also demonstrated shifts in cortical receptive field location and orientation tuning that depend on the relative timing of paired conditioning visual stimuli on the order of tens of milliseconds (Fu, 2002 #35; Yao, 2001 #36; Yao, 2004 #37), consistent with spike-timing-dependent synaptic plasticity (STDP) (Markram, 1997 #30; Bi, 1998 #29). Together, these studies have demonstrated multiple forms of rapid plasticity in adult visual cortex. However, it remains unclear how often these mechanisms are invoked by natural stimuli, and how they enhance visual processing under natural conditions.

The importance of natural stimuli in shaping cortical functions has been demonstrated on much longer time scales. During development, natural visual experience is known to be crucial for the refinement of cortical circuitry and function over days to months (Chapman, 1993 #10; White, 2001 #11) (Li, 2006 #54). Although this refinement is most evident in young animals, experience-dependent improvement of visual cortical

function can occur throughout the lifetime of the animal, as revealed by studies of perceptual learning in adults (Fahle, 2002 #27) (Furmanski, 2004 #28) (Schoups, 2001 #8) (Crist, 2001 #21)(Li, 2004 #42). Since these effects are typically studied over days to months, the immediate impacts of natural stimuli on cortical processing remain largely unexplored.

In the present study, we demonstrate a form of rapid visual cortical modification induced by natural stimuli. A few minutes of repeated stimulation with natural movies, but not white noise or flashed bars, cause a significant improvement of response reliability of cortical neurons. Unlike contrast adaptation, in which repeated stimulation causes a reduction in cortical responses to the adapting stimuli (Maffei, 1973 #30), the increased response reliability is mediated by enhanced cortical responses to subsets of the repeated stimuli. Surprisingly, the repeated movie stimulation also leaves a memory trace in the subsequent spontaneous cortical activity, revealed by an increased similarity between the spontaneous firing patterns and the movie-evoked responses.

Methods

Electrophysiology recording

Animal use procedures were as previously described (Touryan, 2002 #24) and approved by the Animal Care and Use Committee at the University of California, Berkeley. A total of 33 adult cats (2 – 6.5 kg) were used. Single-unit recordings were made in area 17 using tungsten electrodes (A-M Systems); unit isolation was based on cluster analysis of waveforms. Cells were sampled randomly at all laminar locations. For all analyses, we only included cells if their response correlations between different

repeats of the natural movie were above chance level ($\left\langle CC(r_i, \frac{1}{n-1}\sum_{j\neq i} r_j) \right\rangle \geq 0.05$, where i and j represent trial numbers, n is the total number of trials, and $\langle\cdot\rangle$ denotes average across trials); no other criteria were used to select cells. A total of 1274 cells were included in this study (Figure 3.1-4, n = 218; Figure 3.5, n = 228; Figure 3.6-7, n=828).

Visual stimulation

Visual stimuli were generated with a PC computer with a Leadtek Winfast 3D L3100 graphics board and presented with a Viewsonic PT813 monitor (RGB short persistence phosphor, size 40 × 30 cm, refresh rate 119 Hz, maximum luminance 80 cd m^{-2}). Luminance nonlinearities were corrected through software. Each natural movie (720, 365, 265, 186, and 73 consecutive images, for 30.1s, 15.3s, 11.2s, 7.8s, and 3.1s movies, respectively) was selected randomly from a natural scene database (van Hateren, 1998 #1); a total of 94 movies were used. Each image (32 × 32 or 64 × 64 pixels, 7 × 7^o – 16 × 16^o, 2× to 5× receptive field diameter) were updated every 5 refresh frames, corresponding to an effective frame rate of 24 Hz (41.9 ms/frame). Each white noise (8 × 8 pixels) or flashed bar (16 bar positions, at the preferred orientation of the cell) sequence (Figure 3.2) consisted of 720 frames (30.1s). In the blank movie (Figure 3.5 – 3.7) a gray screen (16 cd m^{-2}) was shown in all frames. For the experiment shown in Figure 3.6 & 3.7 using 30.1s, 15.3s, 11.2, 7.8s, or 3.1s natural movies, block M always consisted of 12 repeats of the movie, whereas blocks B1 and B2 each consisted of 12, 24, 36, 48, or 120 repeats of the corresponding blank movie, respectively.

Reliability measure

To measure the response reliability in each trial, we binned the spike trains at the frame rate of the stimulus (41.9 ms), and computed the correlation coefficient (CC) between each repeat r_i and its neighboring 4 repeats $(r_{i-2}+r_{i-1}+r_{i+1}+r_{i+2})/4$. The only exceptions are r_1, r_2, r_{n-1}, *and* r_n, which are correlated with $(r_2+r_3+r_4+r_5)/4$, $(r_1+r_3+r_4+r_5)/4$, $(r_{n-4}+r_{n-3}+r_{n-2}+r_n)/4$, and $(r_{n-4}+r_{n-3}+r_{n-2}+r_{n-1})/4$, respectively.

Surrogate spontaneous signals

For each cell we generated two sets of surrogate spontaneous signals ($R_{B1\_control}$ and $R_{B2\_control}$) by random sampling. Each surrogate signal was averaged from the same number of spike train segments as R_{B1} or R_{B2}, but these segments were selected randomly from the corresponding spike train (Figure 3.7a); 10,000 surrogate signals were generated for each cell. This procedure, while disrupting the periodically recurring temporal patterns, ensured that $R_{B2\_control}$ and $R_{B1\_control}$ were matched to R_{B2} and R_{B1} in mean firing rate and in local temporal correlations (e.g., due to refractory period or bursting). Thus, although in principle changes in the general statistics of spontaneous spike trains following movie stimulation may contribute to the difference between CC (R_{B1}, R_M) and CC (R_{B2}, R_M), converting these CC values to their Z scores based on the distributions of CC ($R_{B1\_control}$, R_M) and CC ($R_{B2\_control}$, R_M) should eliminate these effects.

Results

Improvement of response reliability induced by natural stimuli

Single-unit recordings were made in the primary visual cortex of anesthetized adult cat (Methods) to test the effects of repetitive stimulation with time-varying natural

scenes (movies). Each movie (30.1 s long; Figure 3.1a, Supplementary Movie 1) was repeated 30 times, and the spike trains of the neuron in different repeats ("trials") were compared to assess the reliability of the response and the change in reliability over trials. As shown in Figure 3.1b, spiking of these cortical neurons evoked by natural movies was relatively sparse (Olshausen, 1996 #30), with brief episodes of high spiking probability interspersed among long periods of low spike rate. Within each episode of high spiking probability, there was considerable inter-trial variability in the number of spikes, consistent with the known spiking characteristics of these neurons(Dean, 1981 #27). However, we also observed a reduction of the variability over repeated trials, as quantified by the correlation coefficient (CC) between the time-binned firing rate in each trial (41.9 ms/bin, frame rate of the movie) and the firing rate averaged over its four neighboring trials (Methods). As shown in Figure 3.1b (right panel), CC for the cell exhibited a trend of increase over trials. For the population of cells studied (96 cells, 26 different movies), CC increased steadily over ~10 trials before saturation (Figure 3.2a). This effect was observed regardless of the stimulation history (either drifting gratings or blank screen for several minutes before the natural movie) and over a wide range of bin sizes (data not shown). Thus, repeated exposure to the movies induced a rapid reduction of cortical response variability and hence an improvement in the coding of natural stimuli.

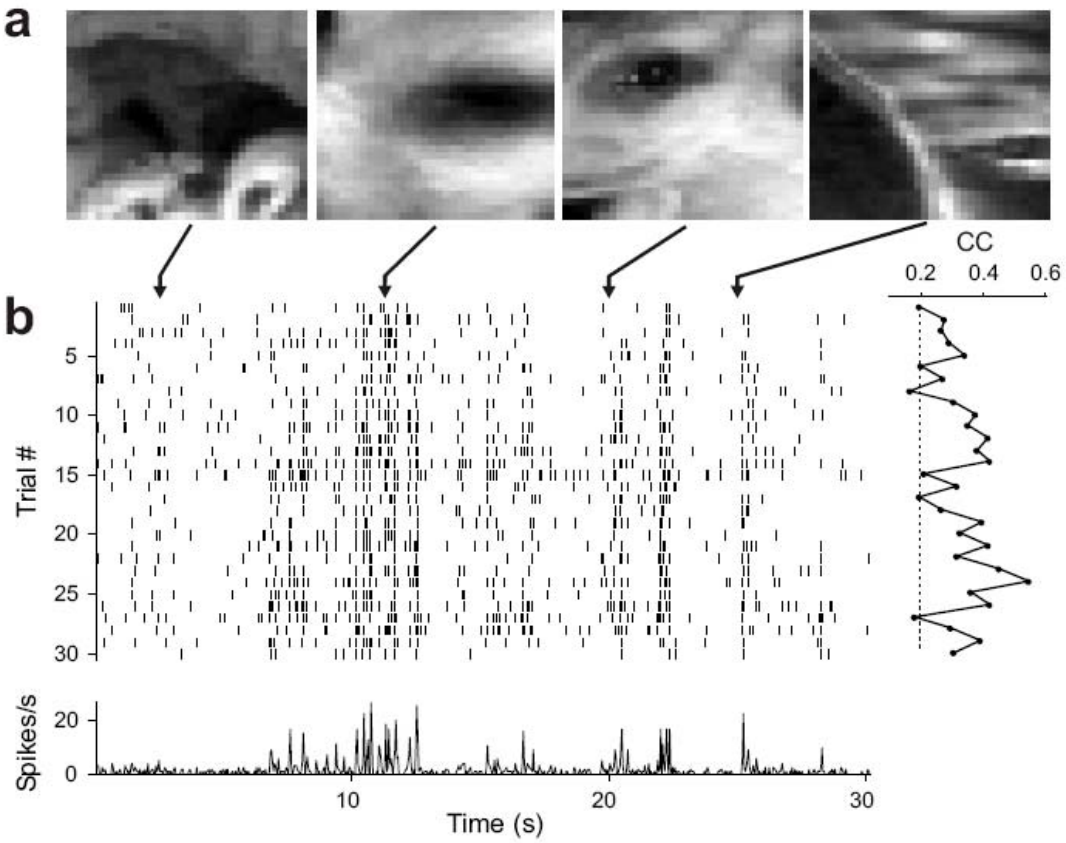

Figure 3.1. Improvement of cortical response reliability over repeated trials of natural movie.

a, Example images from a movie. Arrow, timing of each image.

b, *Left*, Responses of a V1 cell to 30 trials of the movie (raster plot and PSTH). *Right*, CC between response in each trial (binned at 41.9 ms) and mean response of its neighboring 4 trials.

To test whether the observed effect is specific to natural stimuli, we also measured cortical responses to repeated sequences of white noise and flashed bar (at the preferred orientation of each cell) stimuli. As shown in Figure 3.2b, c, these two types of

stimuli did not induce consistent increase in CC over the 30 trials, indicating that the increase in response reliability (Figure 3.2a) is relatively specific to natural stimuli.

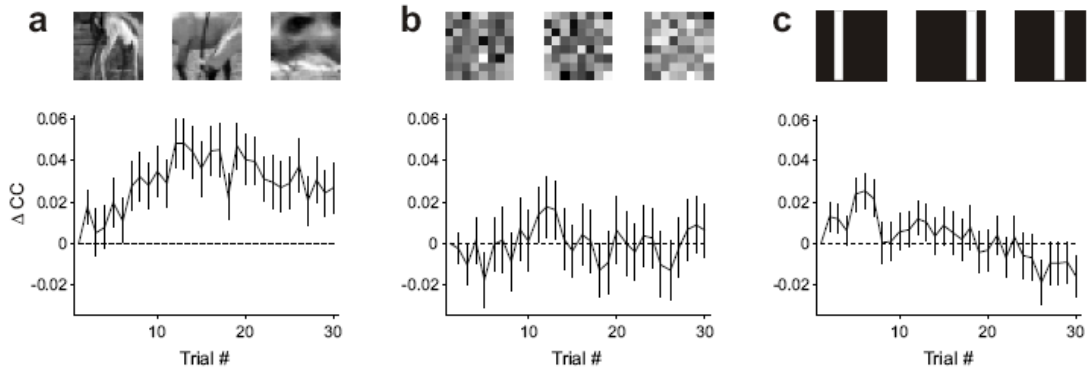

Figure 3.2. Improvement of response reliability is specific to natural stimuli.

a, Change in CC induced by natural stimuli, averaged across 96 cells (26 movies). ΔCC: CC in each trial minus CC in the first trial. Error bar, ± s.e.m. *S*pike trains were binned at the stimulus frame rate (41.9 ms). Increase in CC (ΔCC averaged over trials 11-30) was significant ($p < 0.0001$, Wilcoxon signed rank test).

b, Change in CC induced by white noise, averaged across 46 cells (15 movies). Increase in CC was not significant ($p > 0.5$).

c, Change in CC induced by flashed bars, averaged across 76 cells (10 movies). Increase in CC was not significant ($p > 0.5$).

Selective increase of spiking

Inspection of the spike trains in response to natural stimuli suggested that the improvement of response reliability was associated with a selective increase of spiking during episodes of high firing probability (Figure 3.3a, gray shading). To quantify this

observation, we divided all the time bins in the PSTH of each cell into two groups, based on a threshold (*T*) set at a fraction (e.g., 20%) of the highest amplitude of the PSTH (Figure 3.3b, dashed red line). The time bins in which the PSTH exceeded *T* were defined as "event" bins (red, 14.2 ± 1.6%, s.e.m., of all time bins) and the rest as "non-event" bins (gray). When spiking within each group of bins was examined over trials, we found a marked increase in the number of spikes in the event bins, but much less change in the non-event bins (Figure 3.3c). The time course of the increase in spiking was similar to that of the CC increase (Figure 3.2a). To further examine the selective increase in spiking and to reduce the arbitrariness in choosing a single threshold, we repeated the above analysis with four thresholds (*T1* to *T4*), which divided the time bins into five groups (Figure 3.3d). We found that the percentage increase in spiking increased monotonically with the threshold (Figure 3.3e, f). Thus, repeated presentation of each movie induced a selective increase in the spiking probability in large events, which presumably represent responses to the preferred stimuli of the cell. Notably, repeated presentation of white noise or flashed bar stimuli also induced a preferential increase of spiking in large events, but the level of increase was much lower than that for natural stimuli (Figure 3.3f, dashed and dotted lines).

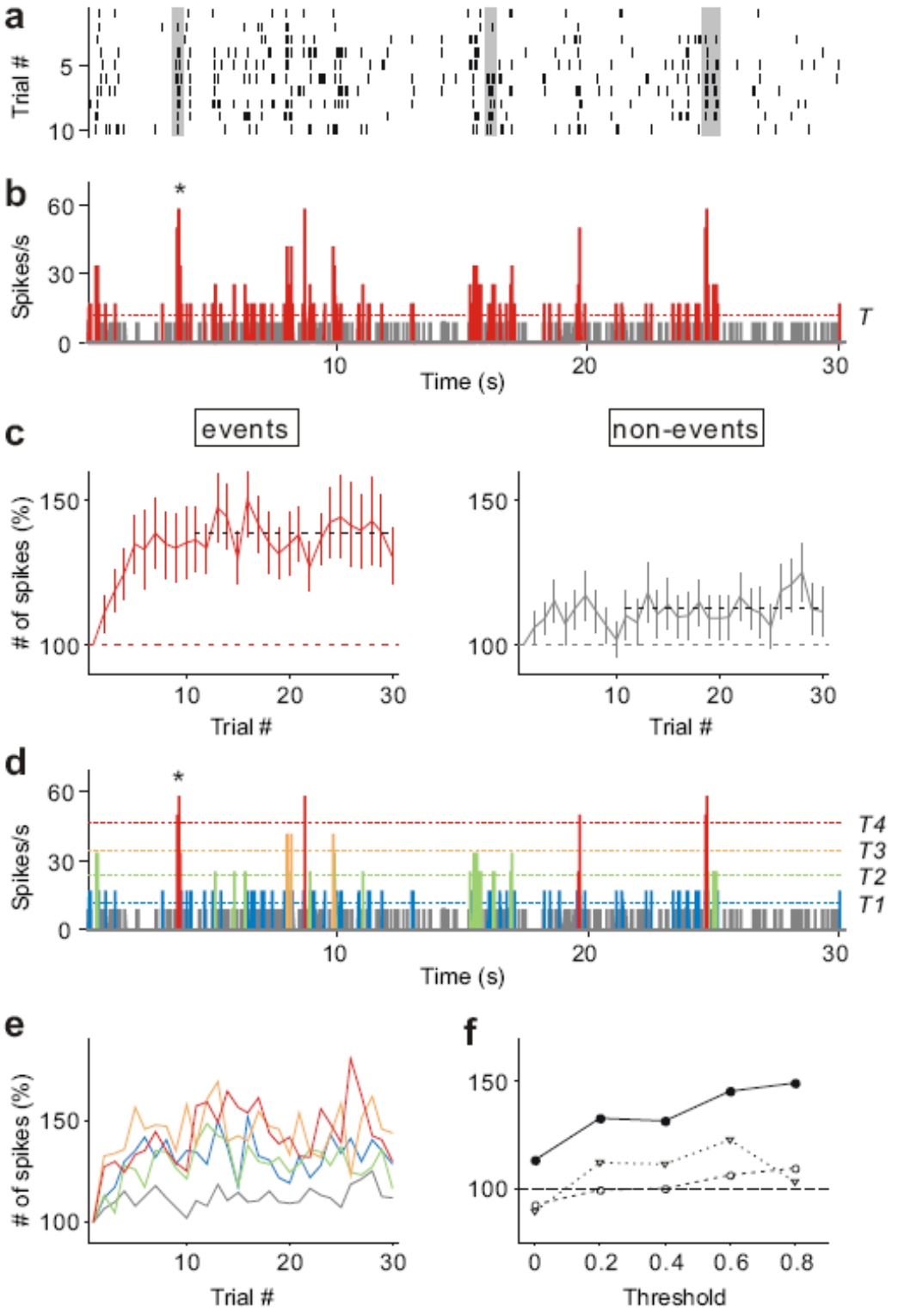
a
Trial #
5
10
b
Spikes/s
60
30
0
*
T
10
20
30
Time (s)
c
events
non-events
# of spikes (%)
150
100
10
20
30
Trial #
d
Spikes/s
60
30
0
*
T4
T3
T2
T1
10
20
30
Time (s)
e
# of spikes (%)
150
100
10
20
30
Trial #
f
150
100
0
0.2
0.4
0.6
0.8
Threshold

Figure 3.3. Selective increase of spiking induced by natural stimuli.

a, Raster plot for the first 10 trials of an example cell evoked by natural movies. Gray shading, high firing rate episodes in which spiking reliability improved over trials.

b, PSTH of the same cell (averaged over 30 trials). Dashed horizontal line, threshold (*T*) at 20% of highest amplitude of PSTH (star). Red and gray, event and non-event bins.

c, Number of spikes normalized by that in the first trial for event (left) and non-event (right) bins, averaged from the same 96 cells in Fig. 3.2a. Error bar, ± s.e.m. Black dotted line, average across trials 11 - 30.

d, Classification of five groups of event bins based on four thresholds. Dashed lines indicate thresholds at 80%, 60%, 40%, and 20% of highest PSTH amplitude. Each group of bins is indicated by a distinct color.

e, normalized spike number over trials in each group of bins (indicated by color) for the 96 cells.

f, normalized spike number averaged across trials 11 – 30 vs. threshold for each group, for natural (filled circle), white noise (triangle), and flashed bar (open circle) stimuli (the same populations of cells shown in Fig. 3.2).

Dependence on sparseness

Why are natural stimuli more effective in inducing the improvement in response reliability? The cortical responses to natural stimuli typically consist of brief episodes of high spiking probability separated by periods of low firing rate (Figure 3.1b, 3.3b), consistent with the notion of sparse coding (Barlow, 1961 #26; Olshausen, 1996 #30). When we compared the distribution of firing rates in response to natural stimuli with the distributions for white noise and random bar stimuli, we found higher probability of both

near-zero and high firing rates but a lower probability of intermediate firing rates (Figure 3.4a), indicating a higher level of response sparseness. Since the improved response reliability is associated with a preferential increase of spiking in large events (Figure 3.3), the effect may depend on a relative abundance of these events (Figure 3.4a, lower plot) and therefore on response sparseness. We measured the sparseness of each cell as $(1-\langle r\rangle^2/\langle r^2\rangle)/(1-1/n)$ (r is firing rate at a given time bin averaged across trials, n is the number of bins, and $\langle\cdot\rangle$ denotes average over all bins) (Vinje, 2000 #31), which quantifies the over-representation of high/low firing rates and under-representation of intermediate rates. As shown in Figure 3.4b, the sparseness of the response to natural stimuli was indeed higher than that for both white noise and flashed bar stimuli. When we plotted the increase in CC against the response sparseness of each cell, we found a significant correlation between them ($p < 0.02$, Figure 3.4c). In particular, the increase in CC was most consistent for cells with sparseness > 0.8 (gray box), but with white noise and flashed bar stimuli the response sparseness rarely reached this level. This suggests that the effectiveness of natural stimuli in inducing the reliability improvement is at least partly due to the higher response sparseness.

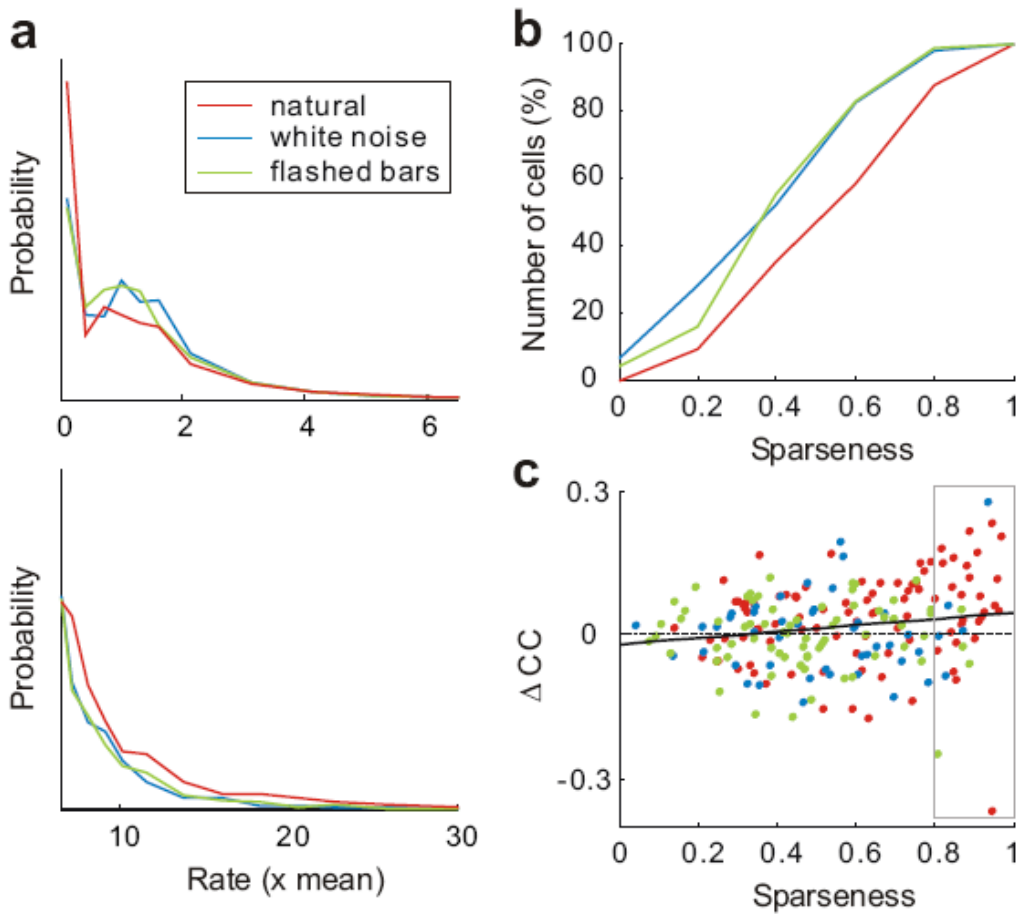

Figure 3.4. Dependence of reliability improvement on response sparseness.

a, Distribution of firing rate in response to natural (red), white noise (blue), and flashed bar (green) stimuli. For each cell, the PSTH was normalized by the mean firing rate, and the histogram (number of bins at each firing rate) is averaged over 96, 46, and 76 cells for natural, white noise, and flashed bar stimuli, respectively (same cells as those in Figs. 3.2 & 3). The distribution at low (< 6.5 × mean, upper plot) and high (≥ 6.5 × mean, lower plot) rates are shown separately; vertical scale of lower plot is 100 × that of upper plot.

b, Cumulative distribution of response sparseness of cortical neurons.

c, ΔCC (averaged across trials 11 – 30) vs. response sparseness. Gray box, cells with sparseness > 0.8.

Persistence of the effect

The improvement of reliability induced by the first few repeats of the movie persisted for at least several minutes in the absence of further stimulation by the same movie. In the experiment shown in Figure 3.5a, we inserted a 6-min resting period (12 repeats of "blank movie", with blank screen in all frames) after the first 12 repeats of a natural movie. The increase in CC over the first 12 trials did not decay significantly over the resting period (Figure 3.5c). Furthermore, inserting 12 repeats of a different movie (movie 2), which evoked distinct firing patterns of the cortical neuron (Figure 3.5b), also did not diminish the increase in CC induced by the first 6 repeats of movie 1 (Figure 3.5d), suggesting that the "memory" of movie 1 was not washed out by a different movie of similar duration.

Reverberation in spontaneous activity

Previous studies in several neural circuits have shown that spontaneous activity exhibits non-random spatiotemporal patterns(Abeles, 1988 #4; Tsodyks, 1999 #17; Dave, 2000 #14; Nadasdy, 1999 #5; Ikegaya, 2004 #6; Louie, 2001 #2; Kenet, 2003 #3)(Foster, 2006 #49), some of which resemble the activity patterns during sensory stimulation(Kenet, 2003 #3; Tsodyks, 1999 #17) or learning-related behavioral tasks(Nadasdy, 1999 #5; Dave, 2000 #14; Louie, 2001 #2)(Foster, 2006 #49). In our study, since the effect of repetitive movie stimulation persisted through a 6-min resting period (Figure 3.5a, c), we searched for a "memory trace" of the movie by testing whether the temporal patterns of spontaneous activity during the resting period exhibit similarity to the responses evoked by the movie.

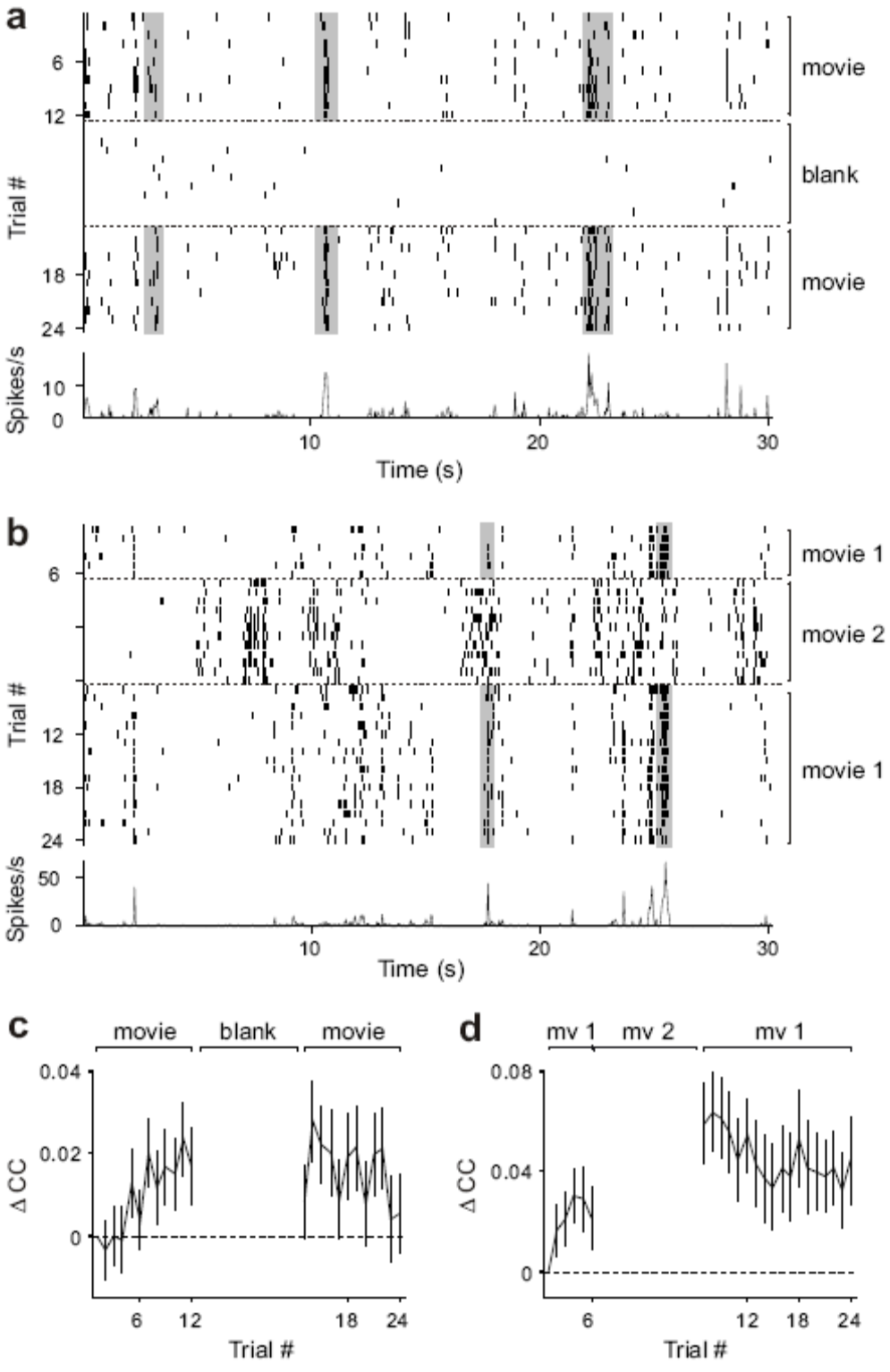
a
movie
blank
movie
Trial #
Spikes/s
Time (s)
b
movie 1
movie 2
movie 1
Trial #
Spikes/s
Time (s)
c
movie
blank
movie
Δ CC
Trial #
d
mv 1
mv 2
mv 1
Δ CC
Trial #

Figure 3.5. Persistence of CC improvement induced by natural movies.

a, Data from an example cell, stimulated by natural (12 trials), blank (12 trials), and the same natural (12 trials) movie. PSTH: mean response to all 24 trials of the natural movie.

b, Another example cell, stimulated by natural movie 1 (6 trials), natural movie 2 (12 trials), and natural movie 1 (18 trials). PSTH: mean response to 24 trials of movie 1.

c, Population summary of ΔCC for natural movie before and after blank movie (experiment in a, n = 148, 41.9ms/bin). Error bar, ± s.e.m.

d, Population summary of ΔCC for movie 1 before and after movie 2 (experiment in b, n = 80). Data shown here are from a different population of cells from those in Figs. 1-4, due to difference in stimulus sequence.

The experiment consisted of three blocks: B1 – M – B2. The M block contained 12 repeats of a natural movie; the length of each movie varied from 3.1s to 30.1s in different experiments. The B1 and B2 blocks each contained ~6 min of "blank movie"; each blank movie had the same length as the natural movie in block M (3.1s to 30.1s), but the number of repeats in each block ranged from 12 to 120. This experiment is analogous to that shown in Figure 3.5a (with blocks M1 – B – M2), except for the difference in the number and sequence of M and B blocks. We tested the hypothesis that, after (but not before) repetition of the natural movie, temporal patterns of the movie-evoked activity continue to reverberate in the cortical circuit, repeating themselves at the same rate as the movie repetition. To detect these patterns in the spontaneous spike trains, which typically exhibit low firing rates (Figure 3.5a), we computed the spontaneous rate signals before and after the movie (R_{B1} and R_{B2}) by averaging over all repeats of the blank movie (i.e.,

PSTH) in each block (Figure 3.6a). We then measured the similarity of R_{B1} and R_{B2} to the movie-evoked response R_M (PSTH, averaged over the 12 repeats in block M) by CC. For the population of cells (Figure 3.6b), we found that CC (R_{B2}, R_M) was significantly higher than CC (R_{B1}, R_M) for short (3.1 s, $p < 0.001$, Wilcoxon signed rank test, $n = 78$) and medium-length (7.8 – 15.3 s, $p < 0.02$, $n = 541$) movies, although not for long movies (30.1s, $p>0.5$, $n = 209$). This indicates that the temporal patterns of spontaneous activity exhibits higher similarity to the movie-evoked response after repeated movie stimulation. This is different from the previously reported similarity between the spatial patterns of spontaneous and evoked cortical activity, which is independent of stimulus history(Kenet, 2003 #3).

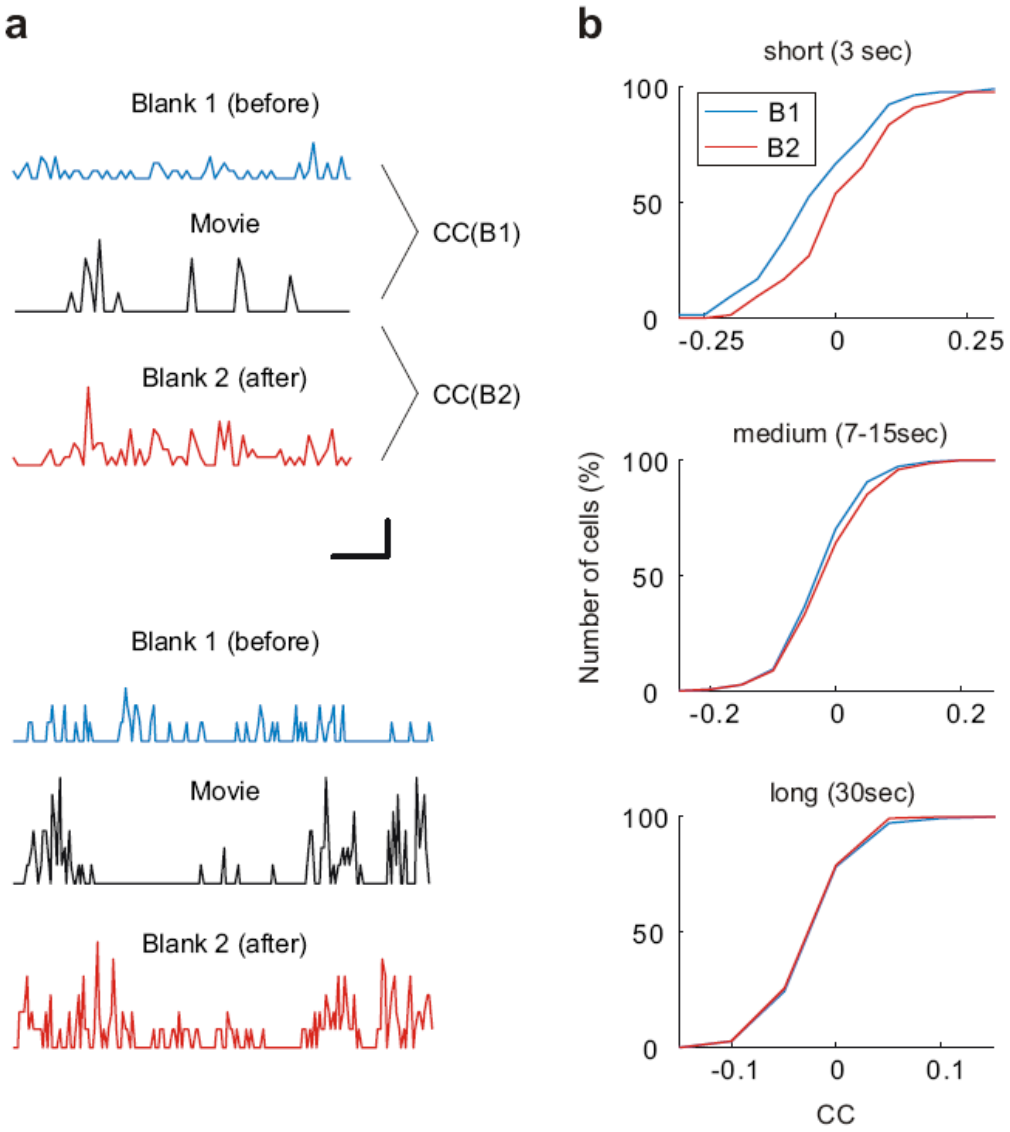

Figure 3.6. Correlation coefficient between spontaneous and visually evoked spiking patterns.

a, Data from two example cells, stimulated by a 3.1s movie (upper) and a 7.8s movie (lower). Shown are PSTHs from B1, M, and B2 blocks. Horizontal scale bar: 0.5s (upper cell) and 1s (lower cell). Vertical scale bar: 1 spikes/s (B1 and B2) and 4 spikes/s (M) for both cells.

b, Cumulative histograms of CC (R_{B1}, R_M) and CC (R_{B2}, R_M) for three groups of cells, stimulated by long (30.1s, n= 209), medium (7.8-15.3s, n= 541), and short (3.1 s, n= 78) movies.

To test whether the increase in CC after movie stimulation is due to changes in the general statistical properties of the spontaneous spike trains (e.g., firing rate, refractory period, burstiness), we performed additional control analyses. First, we generated large numbers of surrogate spontaneous signals ($R_{B1\_control}$ and $R_{B2\_control}$) for each cell by random sampling (Figure 3.7a) of the spike trains in B1 or B2, respectively. Since random sampling preserves the general spiking statistics but disrupts signals that reverberate at the rate of the movie repetition, the distributions of CC ($R_{B1\_control}$, R_M) and CC ($R_{B2\_control}$, R_M) reflect the similarity between spontaneous and evoked activity due to non-specific causes. When CC (R_{B1}, R_M) and CC (R_{B2}, R_M) were converted into Z scores based on their control CC distributions(Louie, 2001 #2) (Methods), we found that the Z score of CC (R_{B2}, R_M) was still significantly higher than that of CC (R_{B1}, R_M) for short ($p < 0.002$) and medium-length ($p < 0.02$) movies (Figure 3.7b). This indicates that the increase in CC is not due to changes in the general statistics of spontaneous firing. To further exclude the possibility that the increase in CC is caused by changes in spontaneous firing rate, we divided the cells into three groups based on the difference in mean firing rate between B1 and B2 (<–10%, between –10% and 10%, and > 10%). We found that the Z score was higher for B2 than for B1 in all three groups, with no correlation between the changes in Z score and in spontaneous firing rate (Figure 3.7c, $p > 0.95$, ANOVA). Finally, we found that the difference between Z scores for B1 and B2

increased with the reliability of the cortical response to the natural stimuli in block M (Figure 3.7d), suggesting that the increase in similarity following the movie stimulation depends on the effectiveness of the movie in driving the cortical neurons.

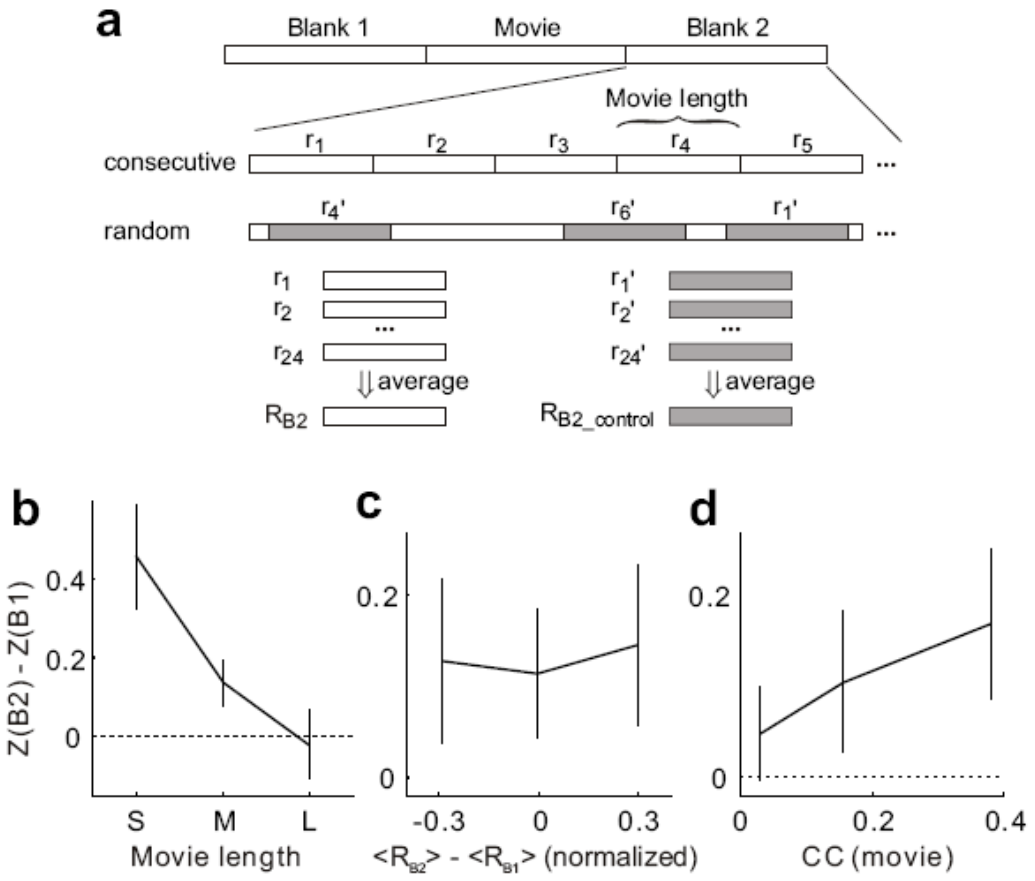

Figure 3.7. Further analysis of CC between spontaneous and visually evoked spiking patterns.

a, Schematic illustration of experimental procedure and definitions of spontaneous rate signal (R_{B2}) and surrogate signals generated by random sampling ($R_{B2\_control}$). The distributions of CC ($R_{B1\_control}$, R_M) and CC ($R_{B2\_control}$, R_M) are used to convert CC (R_{B1}, R_M) and CC (R_{B2}, R_M), respectively, to Z scores.

b, Difference between Z scores in B1 and B2 at different movie lengths. The difference is significant for short (3.1 s, $p < 0.001$, $n = 78$) and medium-length (7.8 – 15.3 s, $p < 0.02$, $n = 541$; for 15.3s movie alone, $p < 0.02$) movies.

c, Difference between Z scores in B1 and B2 vs. normalized change in spontaneous firing rate, $(\langle R_{B1}\rangle - \langle R_{B2}\rangle)/(\langle R_{B1}\rangle + \langle R_{B2}\rangle)$, where $\langle\cdot\rangle$ represents average over the B1 or B2 block.

d, Difference between Z scores in B1 and B2 vs. reliability of the response to the movie, measured by $\left\langle CC(r_i, \frac{1}{n-1}\sum_{j\neq i} r_j)\right\rangle$, where i and j represent trial numbers, n is the total number of trials, and $\langle\cdot\rangle$ denotes average across trials.

Discussion

Our study shows that repetitive stimulation with natural scenes not only induces a rapid improvement in cortical response reliability, but also leaves a memory trace in subsequent spontaneous activity. Repeated exposure to given visual stimuli is known to induce perceptual learning in adult animals over periods of days to weeks, mediated in part by functional modifications of early visual circuits such as V1(Crist, 2001 #21; Schoups, 2001 #8)(Furmanski, 2004 #28) (Li, 2004 #42) (Frenkel, 2006 #43). Our study reveals a new form of learning in cortical coding of natural stimuli that occurs within minutes, similar in rapidity to the learning in locust antennal lobe induced by repeated odor stimulation(Stopfer, 1999 #7). The improvement in response reliability as measured by CC increase is approximately linear over the first ~10 trials, and even a single trial causes a small but significant improvement (Figure 3.2a, $p < 0.05$, Wilcoxon signed rank test). Such a rapid effect may contribute to visual priming, in which recent exposure to a given visual stimulus facilitates its perception in subsequent encounters (Tulving, 1990

#48). Note that our study has only provided the first demonstration of this phenomenon in the primary visual cortex. In future studies, it would be important to determine whether such rapid learning occurs in awake animals under natural visual behavior, during which the same stimulus pattern is rarely repeated multiple times.

Mechanism for the improvement in response reliability

The observed effect is likely to be distinct from contrast adaptation (Maffei, 1973 #30), in which repeated exposure to given stimuli (e.g., sinusoidal gratings) reduces the cortical responses to the adapting stimuli (Saul, 1989 #32; Saul, 1989 #33; Movshon, 1979 #34). Instead, repeated stimulation with natural movies induced an increase of spiking in response to subsets of the repeated stimuli (Figure 3.3). In addition, the increased response reliability lasted for at least 6 min in the absence of further stimulation (Figure 3.5). This is longer than the time course for recovery from contrast adaptation (Sanchez-Vives, 2000 #35), which is thought to be mediated by a reduction in neuronal excitability (Carandini, 1997 #36; Sanchez-Vives, 2000 #35) or short-term synaptic depression (Chance, 1998 #37).

A potential mechanism for the observed effect is Hebbian synaptic plasticity, which is likely to underlie several forms of adult cortical modification induced by minutes of visual stimulation (Eysel, 1998 #34)(Yao, 2001 #39; Yao, 2004 #40; Fu, 2002 #38). In particular, the selective increase of response within episodes of high spiking probability (Figure 3.3) is consistent with the requirement for postsynaptic spiking in STDP (Markram, 1997 #44; Bi, 1998 #45), a robust form of synaptic plasticity in both superficial(Froemke, 2002 #46) and deep (Sjostrom, 2002 #47) layers of the visual cortex.

Patterns of spontaneous activity

Previous studies using voltage-sensitive dye imaging have shown that the spatial patterns of ongoing activity in cat V1 resemble the orientation maps measured with gratings (Kenet, 2003 #3; Arieli, 1996 #15). In our study, similarity between spontaneous and evoked activity was found in the temporal patterns of single neuron firing. A major difference between these findings is that, while the spatial similarity appears to be present in the adult visual cortex independent of the stimulus history, the temporal similarity we have observed emerges after repeated movie stimulation (Figure 3.6). It is possible that both types of similarity result from experience-dependent cortical modification at different time scales: Whereas the temporal similarity represents reverberation of the most recent visual experience, the spatial similarity reflects the long-term impact of visual experience on intracortical connectivity patterns.

The stimulus-induced similarity between spontaneous and visually-evoked cortical activity (Figure 3.6 & 3.7) is reminiscent of the "replay" of learning-related activity in neural circuits mediating episodic (Nadasdy, 1999 #5; Louie, 2001 #2)(Foster, 2006 #49) and sensorimotor(Dave, 2000 #14) learning. In these studies, temporal firing patterns of single or multiple neurons recorded during the learning period are observed in the neural circuit afterwards, either during sleep (Louie, 2001 #2; Nadasdy, 1999 #5; Dave, 2000 #14) or in the awake state immediately after the experience (in this case with reversed sequence) (Foster, 2006 #49). However, there is an important difference between these previously reported replays and the phenomenon shown in the current study. In both the hippocampus and the bird song circuit, replay appears to occur at irregular intervals, and matches between the experience-related and spontaneous activity

patterns were searched for at all temporal shifts. In addition, the spike sequences are often replayed on compressed (Foster, 2006 #49; Nadasdy, 1999 #5) or expanded (Louie, 2001 #2; Dave, 2000 #14) time scales. Our analysis, on the other hand, only identifies patterns recurring at the same rate as the movie repetition, since the probability of matching at arbitrary temporal shifts is represented in the randomly sampled surrogate signals and therefore discounted when CC is converted into the Z score (Figure 3.7).

The mechanism for such periodic replay may involve oscillations in the cortex. For example, slow wave oscillations (0.1 - 1Hz) known to be initiated in the cortex (Steriade, 1993 #50) may be well suited for reverberating temporal sequences lasting for several seconds, the length of replayed sequences we found in the visual cortex (up to ~15s). Another potential mechanism is synaptic modification through STDP (Bi, 1998 #45; Froemke, 2002 #46; Markram, 1997 #44; Sjostrom, 2002 #47). Theoretical studies indicate that STDP is a powerful mechanism for learning temporal sequences (Abbott, 1996 #51; Rao, 2000 #52). Experimentally, learning of temporal patterns has been demonstrated in cultured neuronal networks, which is thought to be mediated by STDP (Bi, 1999 #53). In our study, the repeated movie presentation may selectively strengthen synaptic pathways that propagate spatiotemporal signals matching the visually evoked responses.

In Hebb's postulate (Hebb, 1949 #28), reverberating activity embodying transient memory facilitates the formation of permanent memory through long-term synaptic modification. In our study, the rapid improvement of response reliability following repetitive natural stimulation may represent a first step in the learning of the stimuli. Subsequent reverberation of the activity patterns may facilitate consolidation of the effect

by long-lasting modifications of cortical connectivity. Given its specificity to natural stimuli (Figure 3.2), the effect we observed may contribute to experience-dependent fine-tuning of visual cortical circuits that underlies efficient coding of natural scenes (Attneave, 1954 #40; Barlow, 1961 #41; Simoncelli, 2001 #22) (Felsen, 2005 #23). Furthermore, the finding of reverberating activity in an early sensory circuit such as V1 raises the possibility that reverberation is a prevalent phenomenon in the nervous system that contributes to multiple forms of learning and memory.

References

Gilbert, C. D. Adult cortical dynamics. *Physiol Rev* **78**, 467-485 (1998).

Chapman, B. & Stryker, M. P. Development of orientation selectivity in ferret visual cortex and effects of deprivation. *J Neurosci* **13**, 5251-5262 (1993).

White, L. E., Coppola, D. M. & Fitzpatrick, D. The contribution of sensory experience to the maturation of orientation selectivity in ferret visual cortex. *Nature* **411**, 1049-1052 (2001).

Barlow, H. B. in *Sensory Communication* (ed. Rosenblith, W. A.) 217-234 (MIT Press, Cambridge, MA, 1961).

Dean, A. F. The relationship between response amplitude and contrast for cat striate cortical neurones. *J Physiol* **318**, 413-427 (1981).

Abeles, M. & Gerstein, G. L. Detecting spatiotemporal firing patterns among simultaneously recorded single neurons. *J Neurophysiol* **60**, 909-924 (1988).

Tsodyks, M., Kenet, T., Grinvald, A. & Arieli, A. Linking spontaneous activity of single cortical neurons and the underlying functional architecture. *Science* **286**, 1943-1946 (1999).

Dave, A. S. & Margoliash, D. Song replay during sleep and computational rules for sensorimotor vocal learning. *Science* **290**, 812-816 (2000).

Nadasdy, Z., Hirase, H., Czurko, A., Csicsvari, J. & Buzsaki, G. Replay and time compression of recurring spike sequences in the hippocampus. *J Neurosci* **19**, 9497-9507 (1999).

Ikegaya, Y. et al. Synfire chains and cortical songs: temporal modules of cortical activity. *Science* **304**, 559-564 (2004).

Louie, K. & Wilson, M. A. Temporally structured replay of awake hippocampal ensemble activity during rapid eye movement sleep. *Neuron* **29**, 145-156 (2001).

Kenet, T., Bibitchkov, D., Tsodyks, M., Grinvald, A. & Arieli, A. Spontaneously emerging cortical representations of visual attributes. *Nature* **425**, 954-956 (2003).

Watanabe, T. et al. Greater plasticity in lower-level than higher-level visual motion processing in a passive perceptual learning task. *Nat Neurosci* **5**, 1003-1009 (2002).

Crist, R. E., Li, W. & Gilbert, C. D. Learning to see: experience and attention in primary visual cortex. *Nat Neurosci* **4**, 519-525 (2001).

Schoups, A., Vogels, R., Qian, N. & Orban, G. Practising orientation identification improves orientation coding in V1 neurons. *Nature* **412**, 549-553 (2001).

Stopfer, M. & Laurent, G. Short-term memory in olfactory network dynamics. *Nature* **402**, 664-668 (1999).

Hebb, D. O. *The Organization of Behavior* (Wiley, New York, 1949).

Simoncelli, E. P. & Olshausen, B. A. Natural image statistics and neural representation. *Annu Rev Neurosci* **24**, 1193-1216 (2001).

Touryan, J., Lau, B. & Dan, Y. Isolation of relevant visual features from random stimuli for cortical complex cells. *J Neurosci* **22**, 10811-10818 (2002).

Skottun, B. C. et al. Classifying simple and complex cells on the basis of response modulation. *Vision Res* **31**, 1079-1086 (1991).

van Hateren, J. H. & Ruderman, D. L. Independent component analysis of natural image sequences yields spatio-temporal filters similar to simple cells in primary visual cortex. *Proc. R. So.c Lond. B Biol. Sci.* **265**, 2315-2320 (1998).

Yao, H. and Dan, Y., Stimulus timing-dependent plasticity in cortical processing of orientation. *Neuron* **32**, pp. 315–323. (2001)

Yao, H., Shen, Y. and Dan, Y., Intracortical mechanism of stimulus-timing-dependent plasticity in visual cortical orientation tuning. *Proc. Natl. Acad. Sci. USA* **101**, pp. 5081–5086. (2004)

J. A. Movshon and P. Lennie. Pattern selective adaptation in striate cortical neurones. *Nature* **278**, 850-852 (1979)

Dragoi V, Sharma J, and Sur M. Adaptation-induced plasticity of orientation tuning in adult visual cortex. *Neuron.* 28, 287-298 (2000)

Sanchez-Vives, M.V. and McCormick, D.A. Cellular and network mechanisms of rhythmic recurrent activity in neocortex. Nature Neuroscience, 3: 1027-1034 (2000)

Bi, G.Q. and Poo, M.M., Synaptic modifications in cultured hippocampal neurons: dependence on spike timing, synaptic strength, and postsynaptic cell type. *J. Neurosci.* **18**, pp. 10464–10472. (1998)

Fu, Y.X., Djupsund, K., Gao, H., Hayden, B., Shen, K. and Dan, Y., Temporal specificity in the cortical plasticity of visual space representation. *Science* **296**, pp. 1999–2003.(2002)

Fu, Y.X., Shen, Y., Gao, H. and Dan, Y., Asymmetry in visual cortical circuits underlying motion-induced perceptual mislocalization. *J. Neurosci.* **24**, pp. 2165–2171. (2004)

Markram, H., Lubke, J., Frotscher, M. and Sakmann, B., Regulation of synaptic efficacy by coincidence of postsynaptic APs and EPSPs. *Science* **275**, pp. 213–215. (1997)

Chapter IV. Reverberation of Recent Visual Experience in Spontaneous Cortical Waves

Overview

Spontaneous waves propagating across large cortical areas may play important roles in sensory processing and circuit refinement, but whether and how these waves are modulated by sensory experience remain poorly understood. Here we report that visually evoked activity reverberates in subsequent spontaneous cortical waves. Voltage-sensitive dye imaging of population activity in rat visual cortex showed that following repetitive presentation of a given visual stimulus, spatiotemporal activity patterns resembling the evoked response appear more frequently in the spontaneous waves. This effect is specific to the response pattern evoked by the repeated stimulus, and it persists for several minutes. Such wave-mediated reverberation may contribute to short-term memory and to long-term perceptual learning by consolidating the transient effect of recent sensory experience into long-lasting cortical modifications.

Introduction

Spontaneous cortical activity in the absence of sensory input often exhibits non-random spatiotemporal patterns(Abeles, 1988; Tsodyks, 1999; Kenet, 2003; Fiser, 2004) and may propagate as waves across large cortical areas(Amzica, 1995; Prechtl, 1997; Sanchez-Vives, 2000; Ermentrout, 2001; Petersen, 2003; Ferezou, 2006; Luczak, 2007). Such spontaneous network activity can exert strong influences on sensory evoked responses(Arieli, 1996; Tsodyks, 1999; Fiser, 2004) and play important roles in activity-dependent circuit modifications(Katz, 1996; Weliky, 2000). Furthermore, recent studies showed that spontaneous activity patterns often correspond closely to sensory evoked responses{Kenet, 2003 #3}, raising the possibility that the spatiotemporal properties of spontaneous activity can be shaped by sensory experience.

To address this question, we use voltage-sensitive dye imaging to study spatiotemporal patterns of spontaneous and evoked activity in the visual cortex of anesthetized adult rats. We found that following repetitive presentation of a given visual stimulus, spatiotemporal activity patterns resembling the evoked response appear more frequently in the spontaneous waves. This effect is specific to the response pattern evoked by the repeated stimulus, and it persists for several minutes. Such reciprocal interactions between spontaneous and evoked activity would have important implications for the function of spontaneous activity in sensory processing.

Methods

Anesthetized animal preparation

Animal use procedures were approved by the Animal Care and Use Committee at the University of California, Berkeley. Adult Long-Evans rats (250-400g, n = 23) were anesthetized with pentobarbital (i.p., 60-70mg/kg initially, maintained at 3mg/hr). The body temperature was maintained at 37^{o}C with a regulated heating pad. A 5×5 mm^2 craniotomy and durotomy were performed over the visual cortex. Voltage-sensitive dye RH1838 or RH1691 was dissolved in saline (1mg/ml) and topically applied to the exposed cortex for 2 hr. The cortex was then washed to remove unbound dye and covered with 1.5% agarose and a glass cover slip. Voltage-sensitive dye signals were imaged with a high-speed MiCam Ultima (SciMedia) camera with a 3×3 mm^2 field of view (100×100 pixels). Light from a tungsten filament lamp (12V, 100W, Olympus) was filtered by a 630±30 nm interference filter and reflected down onto the cortex by a 655 nm dichroic mirror (Chroma Technology). Fluorescence signals from the stained cortex were filtered with a 695 nm long-pass filter.

Awake animal preparation

Animal use procedures were approved by the Animal Care and Use Committee at the University of California, Berkeley. Long Evans rats (27-40 days old; 70-120 g, n = 6) were used. Prior to the procedures, animals were handled extensively and accustomed to the restraining setup. Buprenorphine (s.c., 0.05 mg/kg) was administered 1 hr before surgical procedures. The rats were anesthetized using ketamine (i.p., 90mg/kg) and xylazine (10mg/kg) and placed in a standard stereotaxic frame (David Kopf Instruments,

Tujunga, CA). Body temperature was maintained at 36°C–37°C via a heating blanket (Harvard Apparatus, Holliston, MA) during the surgery. Craniotomy and durotomy (4×4 mm^2) were performed over the visual cortex. The exposed cortex was covered with Kwick-Cast (World Precision instruments, Sarasota, FL). A custom-built restrain post, which included a 5×5 mm^2 imaging chamber was then glued to the skull using Relyx Luting Cement (3M ESPE, St. Paul, MN). Dental cement (A-M Systems Inc, Carlsborg, WA) was applied over the restraining post and exposed skull to strengthen the implant. The rat was allowed 1 - 4 days for recovery.

During the imaging session, the rat was anesthetized with 2% isofluorane. The head post was fixed to the head post holder, and the animal was placed inside a custom-made cotton bag that limited its mobility. The Kwick Cast was then removed. Staining was performed as described for the anesthetized animals (Methods). After a few imaging trials under anesthesia, isofluorane was turned off and the animal was allowed to wake up. Animals were considered awake after >20 min and after signs of alertness (e.g., voluntary movement of the limbs or tail and/or reactions to loud sounds) were observed. Imaging experiments proceeded as described for anesthetized animals.

Visual stimulation

Visual stimuli were generated with a PC computer with a NVIDIA GeForce 6600 graphics board and presented with a XENARC 700V LCD monitor (19.7cm × 12.1cm, 960×600 pixels,119 Hz, maximum luminance 16 cd m^{-2}) placed 15 cm from the contralateral eye. Each stimulus was a bright square (30^o) flashed (50 ms, maximum

luminance) at one of the 3 × 3 positions. Spontaneous cortical activity was recorded while the stimulation monitor was dark (< 1.3 cd m^{-2}).

Data analysis

VSD image sequences were analyzed using BV_Analyser (SciMedia) and custom-written Matlab software. We corrected for bleaching but not for heartbeat artifacts since they were small.

To measure the similarity between the spontaneous activity (~10 s/session) and each evoked response (150 - 300 ms), we averaged the spatiotemporal signals in response to 2-4 trials of each visual stimulus and used it as a sliding template to identify similar patterns in spontaneous activity. The correlation coefficient (CC) between the template and the segment of spontaneous recording centered at time *t*, CC(*t*), was plotted for each spontaneous recording session. We found that each spontaneous wave corresponded to a peak in CC(*t*), with the magnitude of CC reflecting the similarity between each spontaneous wave and the template in both initiation site and propagation path (e.g., CC > 0.7 indicates high similarity, see Figure 4.2, ▲▲). Thus, to quantify the effect of repeated visual stimulation on the spontaneous waves, we first used a threshold of 0.4 for CC(*t*) to select time periods corresponding to spontaneous waves (but results are very similar for thresholds between 0.3 and 0.6). Then, we computed the distribution of CCs only during these periods, and compared the mean of the CC distribution before and after training. Note that without using the threshold, the mean of CC(*t*) over the entire spontaneous recording is strongly affected by the frequency of spontaneous waves, since CC(*t*) during waves are almost always positive, while CC(*t*) during the resting period is

near 0. Using the threshold essentially eliminated the confounding effect of wave frequency, since the number of waves included in the analysis merely affects the sample size without changing the mean of the CC distribution.

As an alternative method, we also directly compared the number of spontaneous waves matching the evoked template before and after training. We again used a threshold of 0.4 for CC(t) to identify spontaneous waves. Another threshold T ($T > 0.4$) was then used to define a match to the template. The number of matches was normalized by the total number of waves in each session (to eliminate the effect of wave frequency). The difference in the percentage of matches before and after training was plotted as a function of T (Figure 4.2d).

Results

Spontaneous and evoked waves

Voltage-sensitive dye imaging was used to study spatiotemporal patterns of spontaneous and evoked activity in the visual cortex of anesthetized adult rats (Figure 4.1a). In the absence of visual stimulation, spontaneous activity initiated at random locations at a frequency of 0.5 – 4 Hz and propagated as waves across several millimeters of the cortical surface (Figure 4.1b, upper panel, Supplementary Movie 1). These waves propagated in various directions (Figure 4.1b, white lines) with a mean speed of 16 ± 4.3mm/s (s.d., Figure 4.1d), comparable to the spontaneous waves observed in other sensory cortical areas *in vivo*(Petersen, 2003; Ferezou, 2006; Luczak, 2007). We also measured the cortical responses to a set of visual stimuli, each of which was a bright square (~30^o visual angle) briefly flashed (50ms) at one of nine positions in the

contralateral visual field (Figure 4.1a). Each stimulus also evoked a wave of activity (Figure 4.1b, lower panel, Supplementary Movie 2)(Prechtl, 1997; Roland, 2006; Ferezou, 2006), which initiated 50-100 ms following the stimulus onset and propagated at a mean speed of 10 ± 4.7 mm/s (s.d., Figure 4.1d). However, unlike the spontaneous waves with random initiation sites and variable propagation directions, the evoked waves were much more reproducible. For each of the nine stimulus positions, the wave was initiated at a fixed cortical location organized retinotopically (Figure 4.1c), and the propagation path (Figure 4.1b, white lines) was highly reproducible across trials. Thus, the spatiotemporal pattern of each evoked wave conveyed substantial information about the visual stimulus.

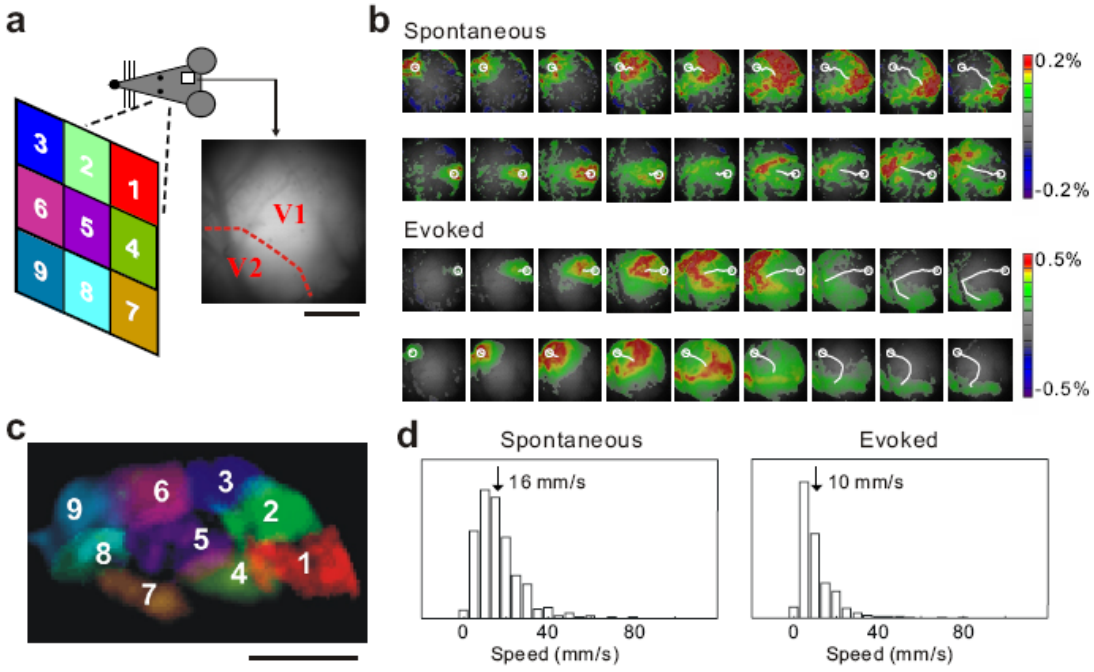

Figure 4.1. Spontaneous and evoked waves in rat visual cortex.

a, Schematic illustration of visual stimulation and cranial window for VSD imaging. Positions for visual stimulation are marked with numbers and colors. *Top right*, image of visual cortex. Red dashed line, approximate V1/V2 border.

b, Examples of spontaneous and visually evoked waves, shown in 20ms intervals. VSD signal was color coded (warm color indicates depolarization), with scale bar shown on right. *Top*, two examples of spontaneous waves. *Bottom*, waves evoked by stimuli at positions 1 & 9. White circle, initiation site measured as center of mass of VSD signal in the first frame. White line, wave trajectory by connecting the centers of mass of consecutive frames.

c, Onset of waves evoked by the nine stimuli (retinotopy), with colors and numbers corresponding to a.

d, Wave speed distributions.

Effect of repeated visual stimulation on spontaneous waves

Consistent with a previous finding in the visual cortex(Kenet, 2003), some of the spontaneous waves resembled visually evoked responses (Figure 4.2a, indicated by ▲). This similarity could reflect the intrinsic cortical connectivity or the long-term impact of previous visual experience. We wondered whether repeated visual stimulation could leave an immediate memory trace in subsequent spontaneous activity. We presented 50 flashes (0.6 Hz) at one of the nine stimulus positions (referred to as the "training stimulus") and compared the spontaneous waves before and after the training with respect to their similarity to the training-evoked wave. Immediately after the training, we found an increase in the number of spontaneous waves that resembled the training-evoked wave in initiation site and propagation path (Figure 4.2a, b). To quantify the similarity between the spontaneous and evoked waves, we used the evoked wave as a spatiotemporal template and computed the correlation coefficients (CC) between the spontaneous activity and this template (see Methods). As shown in Figure 4.2c, the mean CC immediately after training was significantly higher than that before training ($p < 10^{-5}$,

Wilcoxon signed rank test, n = 36), suggesting an increase in similarity between the spontaneous and the evoked waves. In addition to the mean CC, we also compared the percentage of spontaneous waves matched to the template before and after training, and found a significant increase over a range of CC thresholds used to define matches (Figure 4.2d). Notably, we found no significant difference in the frequency of spontaneous waves before and after training (change: $7.8 \pm 5.9\%$, s.e.m., $p > 0.6$, Wilcoxon signed rank test, n = 36), indicating that the increase in similarity was not accompanied by changes in the overall cortical excitability. A similar effect was also observed using a moving bar as the training stimulus (increase in mean CC, $p < 0.05$, n = 22). Such an increase in the similarity between the spontaneous and the training-evoked waves is reminiscent of the notion of network reverberation(Lorente de No, 1938; Hebb, 1949), in which activity patterns evoked by sensory stimuli continue to reverberate in the neural circuits after termination of the stimulus. Interestingly, related phenomena have been described recently in the honeybee antennal lobe using Ca^{2+} imaging(Galan, 2006) and in cat V1 using single-unit recordings(Yao, 2007).

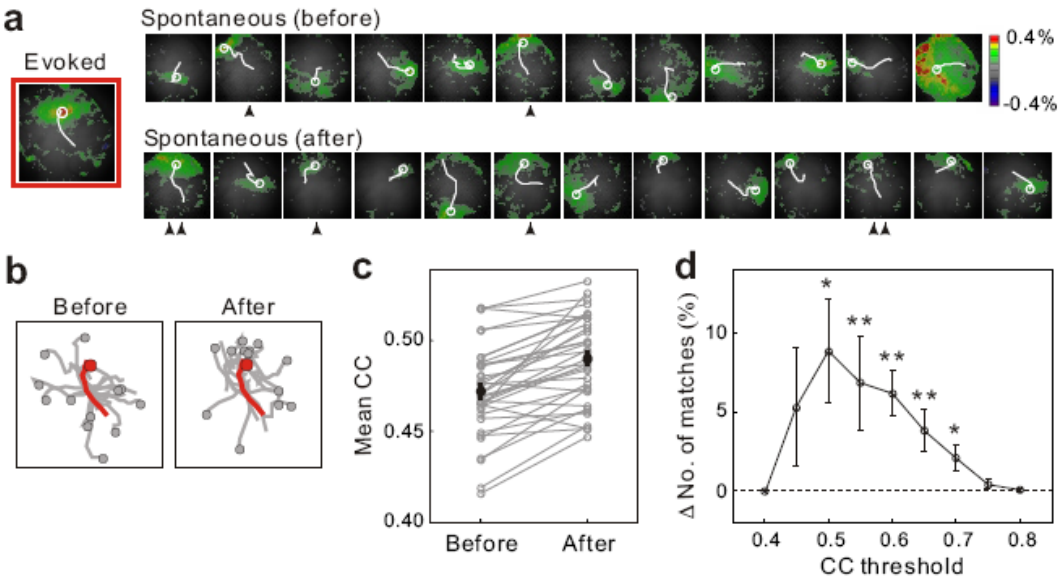

Figure 4.2. Effect of repeated visual stimulation on spontaneous waves.

a, Spontaneous waves immediately before and after training (~10s/session). Each image shows initial frame of a wave. Initiation site and propagation trajectory are indicated by white circle and line. *Left*, Evoked wave in response to the training stimulus. Spontaneous waves matched to the template are indicated; ▲, CC>0.6; ▲▲, CC>0.7.

b, Superposition of the initiation sites and propagation paths for all spontaneous waves before and after training (gray) and the training-evoked wave (red).

c, Mean of CC distribution before and after 50 repeats of the training stimulus. Each pair of gray circles (connected by line) represents one experiment. Black circle: population mean. Error bar: ± s.e.m.

d, Difference in the percentage of matched waves before and after training plotted as a function of threshold for match (*, $p < 0.05$; **, $p < 0.01$).

Specificity of the effect to the training pattern

We next tested whether the reverberation induced by repeated stimulation at one position generalizes to the responses for other positions. We found that following training, the CC also increased for some of the untrained stimulus positions. However, we often noticed similarity between the spatiotemporal response patterns evoked by different stimuli (e.g., Figure 4.3a, middle and right positions in top row), suggesting that the increase in CC for untrained positions could be partly due to the similarity between templates. To address this confounding effect, we measured the dissimilarity between each untrained template and the trained template as $1 - CC(Template_{trained}, Template_{untrained})$. As shown in Figure 4.3b, the untrained templates exhibited varying degrees of dissimilarity to the trained template. Figure 4.3c shows the change in CC between the spontaneous waves and each evoked template as a function of its dissimilarity to the trained template. The change in CC decreased monotonically with the dissimilarity, suggesting that the observed generalization largely reflects the similarity between templates rather than a change in the overall state of the cortical network. Furthermore, when we presented the same number of flashes but randomly distributed over the nine positions, we found no increase in CC between the spontaneous waves and any of the evoked templates (Figure 4.2c, $p > 0.6$, $n = 22$). This further supports the specificity of the reverberation effect.

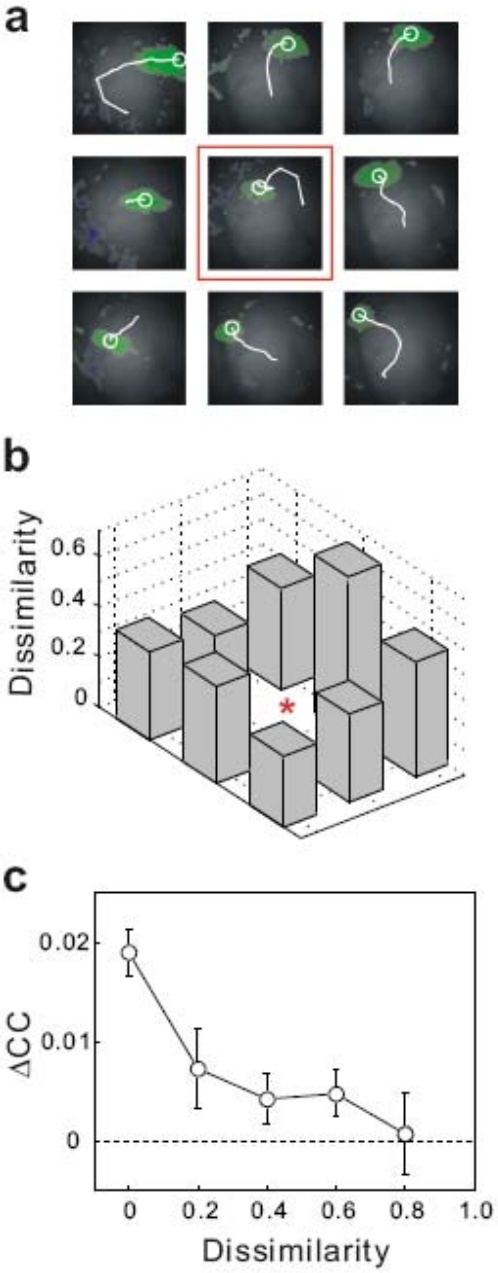

Figure 4.3. Specificity of the effect to the training pattern.

a, Initiation sites and trajectories of waves evoked by the nine stimuli in an example experiment. Red box indicates response to the training stimulus.

b, Dissimilarity (1-CC) between the wave evoked by each non-training stimulus to that evoked by the training stimulus. Red star, dissimilarity for the training stimulus (= 0).

c, Change in mean CC between spontaneous waves and all evoked templates plotted against the dissimilarity between the untrained and trained templates. Circle, mean ΔCC, Error bar, ± s.e.m. n = 11 to 69.

Induction and decay time course of the effect

Finally, we examined the time course for the induction and persistence of the effect. Figure 4.4a shows the increase in CC immediately after training as a function of the number of training flashes. An effect was detectable after 25 flashes, and its magnitude increased monotonically with the number of repeats. To measure the persistence of the effect, we measured the CC between the trained template and the spontaneous waves at different time periods following training. As shown in Figure 4b, following 50 flashes, the effect decayed with a time constant of 1.0 min, and reached the baseline within ~3 min. Increasing the amount of training to 125 flashes not only increased the initial magnitude of the effect, but also increased the decay time constant to 3.8 min. Thus, the reverberation effect can last for several minutes, with its persistence depending on the amount of training.

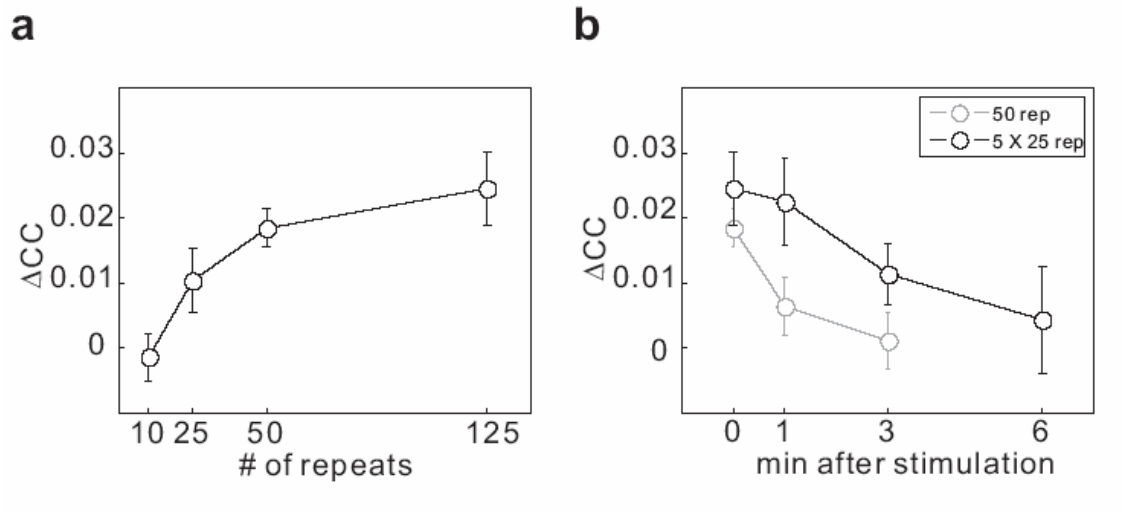

Figure 4.4. Induction and decay time course of the effect.

a, ΔCC vs. number of training stimuli (n = 20 to 32).

b, Persistence of ΔCC induced by 50 (gray) and 125 (black, given in 5 blocks, with 40s between blocks) training stimuli (n = 30 and 20 for gray and black lines, respectively).

Discussion

Our finding is consistent with the notion of reverberating activity proposed by Lorente De No(Lorente de No, 1938) and Hebb(Hebb, 1949). Reactivation of learning-related neural activity has also been shown in the hippocampus(Wilson, 1994; Nadasdy, 1999; Louie, 2001), neocortex(Hoffman, 2002; Ribeiro, 2004; Ji, 2007), and birdsong circuits(Dave, 2000) during sleep. Our study shows that visual stimuli can leave an immediate trace in the spontaneous activity in the first stage of cortical processing. Given its specificity (Figure 4.3), this effect could serve as a mechanism for short-term learning effects such as visual priming(Tulving, 1990), in which recent exposure to a particular stimulus facilitates its perception in subsequent encounters. Furthermore, our results point to the importance of cortical waves in network reverberation. Waves are natural modes of information propagation in large neuronal networks(Ermentrout, 2001), and they may play important roles in information processing(Jancke, 2004; Lee, 2005; Rubino, 2006; Roland, 2006) and memory storage(Marshall, 2006). Although the current study was performed in anesthetized animals, we also observed both spontaneous and evoked waves in the visual cortex of awake rats (Supplementary Movies 3-5), suggesting that they are widespread in early sensory processing(Prechtl, 1997; Lee, 2005; Ferezou, 2006; Luczak, 2007). The correlated activation of a large number of neurons during waves is also likely to facilitate long-term synaptic modifications(Bi, 2001). Thus, the reverberation of sensory-evoked activity in spontaneous cortical waves may not only serve as a carrier for short-term memory, but also promote long-lasting modifications of cortical circuitry

underlying perceptual learning and efficient coding of sensory stimuli.

References

Abeles, M. & Gerstein, G. L. Detecting spatiotemporal firing patterns among simultaneously recorded single neurons. *Journal of Neurophysiology* 60, 909-924 (1988).

Tsodyks, M., Kenet, T., Grinvald, A. & Arieli, A. Linking spontaneous activity of single cortical neurons and the underlying functional architecture. *Science* 286, 1943-1946 (1999).

Kenet, T., Bibitchkov, D., Tsodyks, M., Grinvald, A. & Arieli, A. Spontaneously emerging cortical representations of visual attributes. *Nature* 425, 954-956 (2003).

Fiser, J., Chiu, C. & Weliky, M. Small modulation of ongoing cortical dynamics by sensory input during natural vision. *Nature* 431, 573-578 (2004).

Amzica, F. & Steriade, M. Short- and long-range neuronal synchronization of the slow (< 1 Hz) cortical oscillation. *J Neurophysiol* 73, 20-38 (1995).

Prechtl, J. C., Cohen, L. B., Pesaran, B., Mitra, P. P. & Kleinfeld, D. Visual stimuli induce waves of electrical activity in turtle cortex. *Proc Natl Acad Sci U S A* 94, 7621-6 (1997).

Sanchez-Vives, M. V. & McCormick, D. A. Cellular and network mechanisms of rhythmic recurrent activity in neocortex. *Nat Neurosci* 3, 1027-34 (2000).

Ermentrout, G. B. & Kleinfeld, D. Traveling electrical waves in cortex: insights from phase dynamics and speculation on a computational role. *Neuron* 29, 33-44 (2001).

Petersen, C. C., Hahn, T. T., Mehta, M., Grinvald, A. & Sakmann, B. Interaction of sensory responses with spontaneous depolarization in layer 2/3 barrel cortex. *Proc Natl Acad Sci U S A* 100, 13638-43 (2003).

Ferezou, I., Bolea, S. & Petersen, C. C. Visualizing the cortical representation of whisker touch: voltage-sensitive dye imaging in freely moving mice. *Neuron* 50, 617-29 (2006).

Luczak, A., Bartho, P., Marguet, S. L., Buzsaki, G. & Harris, K. D. Sequential structure of neocortical spontaneous activity in vivo. *Proc Natl Acad Sci U S A* 104, 347-52 (2007).

Arieli, A., Sterkin, A., Grinvald, A. & Aertsen, A. Dynamics of ongoing activity: explanation of the large variability in evoked cortical responses. *Science* 273, 1868-1871 (1996).

Katz, L. C. & Shatz, C. J. Synaptic activity and the construction of cortical circuits. *Science* 274, 1133-8 (1996).

Weliky, M. Correlated neuronal activity and visual cortical development. *Neuron* 27, 427-30 (2000).

Lorente de No, R. Analysis of the activity of the chains of internuncial neurons. *J Neurophysiol* 1, 207-244 (1938).

Hebb, D. O. *The Organization of Behavior* (Wiley, New York, 1949). 17. Tulving, E. & Schacter, D. L. Priming and human memory systems. *Science* 247, 301-6 (1990). 18.

Bi, G. & Poo, M. Synaptic modification by correlated activity: Hebb's postulate revisited. *Annu Rev Neurosci* 24, 139-66 (2001).

Roland, P. E. et al. Cortical feedback depolarization waves: a mechanism of top-down influence on early visual areas. *Proc Natl Acad Sci U S A* 103, 12586-91 (2006).

Galan, R. F., Weidert, M., Menzel, R., Herz, A. V. & Galizia, C. G. Sensory memory for odors is encoded in spontaneous correlated activity between olfactory glomeruli.

Neural Comput 18, 10-25 (2006).

Yao, H., Shi, L., Han, F., Gao, H. & Dan, Y. Rapid learning in cortical coding of visual scenes. *Nat Neurosci* in press (2007).

Wilson, M. A. & McNaughton, B. L. Reactivation of hippocampal ensemble memories during sleep. *Science* 265, 676-9 (1994).

Nadasdy, Z., Hirase, H., Czurko, A., Csicsvari, J. & Buzsaki, G. Replay and time compression of recurring spike sequences in the hippocampus. *J Neurosci* 19, 9497-9507 (1999).

Louie, K. & Wilson, M. A. Temporally structured replay of awake hippocampal ensemble activity during rapid eye movement sleep. *Neuron* 29, 145-156 (2001).

Hoffman, K. L. & McNaughton, B. L. Coordinated reactivation of distributed memory traces in primate neocortex. *Science* 297, 2070-3 (2002).

Ribeiro, S. et al. Long-lasting novelty-induced neuronal reverberation during slow-wave sleep in multiple forebrain areas. *PLoS Biol* 2, E24 (2004).

Ji, D. & Wilson, M. A. Coordinated memory replay in the visual cortex and hippocampus during sleep. *Nat Neurosci* 10, 100-7 (2007).

Dave, A. S. & Margoliash, D. Song replay during sleep and computational rules for sensorimotor vocal learning. *Science* 290, 812-816 (2000).

Jancke, D., Chavane, F., Naaman, S. & Grinvald, A. Imaging cortical correlates of illusion in early visual cortex. *Nature* 428, 423-426 (2004).

Lee, S. H., Blake, R. & Heeger, D. J. Traveling waves of activity in primary visual cortex during binocular rivalry. *Nat Neurosci* 8, 22-3 (2005).

Rubino, D., Robbins, K. A. & Hatsopoulos, N. G. Propagating waves mediate

information transfer in the motor cortex. *Nat Neurosci* 9, 1549-57 (2006).

Marshall, L., Helgadottir, H., Molle, M. & Born, J. Boosting slow oscillations during sleep potentiates memory. *Nature* 444, 610-3 (2006).

Chapter V. Conclusion and closing marks

Overview

The described characterizations of receptive field subunits in awake animal V1 and rapid learning induced plasticity in adult visual cortex provided new insights about mechanisms and properties of visual coding. This chapter concludes the thesis with a general summary and notes on future directions.

Summary of findings

This thesis began with an introductory chapter describing two fundamental levels of visual coding: receptive field characterization of single neuron and activity dependent visual plasticity in cortical circuit. At the level of individual cell, a crucial step in understanding the function of a neural circuit in visual processing is to know what stimulus features are represented in the spiking activity of the neurons. For neurons with complex, nonlinear response properties, characterization of feature representation requires measurement of their responses to a large ensemble of visual stimuli and an analysis technique that allows identification of relevant features in the stimuli. After measuring RF structures quantitatively, we can validate such RF models and predict the responses of a given neuron to arbitrary visual stimuli. On the other hand, sensory experiences could often refine cortical network. Experience-dependent synaptic plasticity is a fundamental organizing principle for neural system. Particularly in visual cortex, visual stimulation can modify cortical circuitry and response properties on multiple time scales. Therefore, it is essential to study both RFs and plasticity in order to understand the fundamental principles of visual coding. Two robust techniques were described and applied in this thesis to address these questions respectively. Spike triggered covariance (STC) has been used effectively to estimate the subunits of RFs of individual cell from their response to white noise stimuli. And a robust *in vivo* brain imaging method (voltage-sensitive dye imaging) was described to measure the spatial-temporal activity patterns of cortical circuit.

The second chapter of this thesis began by revealing the spatial structures of receptive fields in the awake monkey V1. We found multiple excitatory and suppressive subunits including one or two dominant excitatory subunits as described by the standard model for most of the cells. STC analysis has allowed identification of two additional groups of subunits: the non-dominant excitatory and suppressive subunits, whose contributions to cortical responses are weaker than the dominant component, at least under white noise stimulation. The non-dominant excitatory subunits are more dispersed spatially but overlap substantially with the dominant component in the frequency spectrum, and they contribute to response invariance with respect to small changes in stimulus orientation, position, and frequency. In contrast, the suppressive subunits overlap with the dominant component spatially but are complementary in the frequency spectrum. They are likely to mediate suppression of the responses to "antagonistic" visual features, including those at the orthogonal orientation or opposite motion direction (Rust et al., 2005). Invariance and selectivity of neuronal responses are both important for visual processing. Together, the excitatory and suppressive subunits form a compact description of neuronal RFs in awake monkey V1, allowing prediction of the responses to arbitrary stimuli.

The third chapter then examined a form of rapid plasticity in cat visual cortex induced by repeated natural stimulation. We show that repetitive exposure with movies of natural scenes induces a rapid improvement of response reliability, an effect largely absent with white noise and flashed bar stimuli. The improved reliability can be accounted for by a selective increase in spiking evoked by preferred stimuli, and the magnitude of improvement depends on the sparseness of the response. The increase in

reliability persists for at least several minutes in the absence of further movie stimulation. A potential mechanism for the observed effect is Hebbian synaptic plasticity, which is likely to underlie several forms of adult cortical modification induced by minutes of visual stimulation. In particular, the selective increase of response within episodes of high spiking probability is consistent with the requirement for postsynaptic spiking in STDP (Markram, 1997; Bi, 1998), a robust form of synaptic plasticity in both superficial(Froemke, 2002) and deep (Sjostrom, 2002) layers of the visual cortex. During this period, there is detectable reverberation of the movie-evoked responses in the spontaneous spiking activity. The stimulus-induced similarity between spontaneous and visually-evoked cortical activity is reminiscent of the “replay” of learning-related activity in neural circuits mediating episodic (Nadasdy, 1999; Louie, 2001)(Foster, 2006) and sensorimotor(Dave, 2000) learning. However, our analysis, on the other hand, only identifies patterns recurring at the same rate as the movie repetition. The mechanism for such periodic replay may involve oscillations in the cortex. For example, slow wave oscillations (0.1 - 1Hz) known to be initiated in the cortex (Steriade, 1993) may be well suited for reverberating temporal sequences lasting for several seconds, the length of replayed sequences we found in the visual cortex (up to ~15s). Another potential mechanism is synaptic modification through STDP (Bi, 1998; Froemke, 2002; Markram, 1997; Sjostrom, 2002). In our study, the repeated movie presentation may selectively strengthen synaptic pathways that propagate spatiotemporal signals matching the visually evoked responses.

The forth chapter investigated whether and how spontaneous activity is modulated by sensory experience in neural circuit by using voltage-sensitive dye imaging. We report

that visually evoked activity reverberates in subsequent spontaneous cortical waves. Voltage-sensitive dye imaging of population activity in the rat visual cortex showed that following repetitive presentation of a given visual stimulus, spatiotemporal activity patterns resembling the evoked response appear more frequently in the spontaneous waves. This effect is specific to the cortical response pattern evoked by the repeated stimulus, and it persists for several minutes. Such "reverberation" of visually evoked responses may contribute to transient perceptual memory. Furthermore, since correlated neuronal activity during waves is likely to be conducive to long-term synaptic modifications, wave-mediated reverberation may contribute to perceptual learning by consolidating the transient effect of recent sensory experience into long-lasting cortical modifications.

Future directions

The experiments described in this thesis seem to raise more questions than they answer. There are some obvious experiments that could be performed; many of these are controls and further evidence for some of the ideas suggested in this thesis.

Receptive field mapping

Our results have shown that STC analysis is highly effective for characterizing the neuronal RF subunits in awake monkey V1. While the current study is performed with white noise stimuli during a simple fixation task, future studies using similar analysis techniques will allow us to examine the RF properties under more naturalistic visual stimulation (David et al., 2004; Touryan et al., 2005) and behavioral conditions. These studies may reveal novel RF properties related to natural scene statistics (Felsen et al.,

2005; Sharpee et al., 2006) and task-dependent top-down modulation of cortical processing (Fritz et al., 2003; Li et al., 2004).

Reverberation of sensory experience

In our study, the finding of reverberating activity in an early sensory circuit such as V1 raises the possibility that reverberation is a prevalent phenomenon in the nervous system that contributes to multiple forms of learning and memory. Several other questions related to this phenomenon remain to be answered. For example, what is the relationship of the reverberating spiking activity in cat V1 and reverberating wave patterns in rat V1? It is likely that some of the differences are due to the difference in measuring techniques. However, cortical waves which are prevalent in rat V1 are not obvious in cat V1 reported by several other VSDI studies in cat. And the periodicity of reverberation observed in cat V1 is absent in the rat experiment, indicating different mechanisms might be involved.

The underlying mechanisms of such reverberations also require further investigation. These issues raise the question of what determines the extent of such phenomenon in the first place. Further pharmacological experiments may reveal more insights about the underlying mechanisms. For example, NMDAR, which is shown to determine the time window for LTP in most studies, might be involved in the phenomenon described in our study.

Lastly, these experiments were performed mostly on anesthetized animals. The next step will be to extend current study to the awake animals. Currently we were able to observe wave activities in the awake head-fixed rat. It will be crucial to examine if the

same phenomenon can be observed in the awake animals. The roles of attention, neuromodulation, sleep and anesthesia are certainly important factors for any type of learning and memory forming.

References

Rust, N. C., Schwartz, O., Movshon, J. A., and Simoncelli, E. P. (2005). Spatiotemporal elements of macaque v1 receptive fields. Neuron *46*, 945-956.

Touryan, J., Felsen, G., and Dan, Y. (2005). Spatial structure of complex cell receptive fields measured with natural images. Neuron *45*, 781-791.

Markram, H., Lubke, J., Frotscher, M. and Sakmann, B., Regulation of synaptic efficacy by coincidence of postsynaptic APs and EPSPs. *Science* **275**, pp. 213–215. (1997)

Froemke, R.C. and Dan, Y. Spike timing-dependent synaptic modification induced by natural spike trains. *Nature* 416, 433-438. (2002)

M Steriade, DA McCormick, and TJ Sejnowski, Thalamocortical oscillations in the sleeping and aroused brain *Science*:Vol. 262.(1993)

Bi, G.Q. and Poo, M.M., Synaptic modifications in cultured hippocampal neurons: dependence on spike timing, synaptic strength, and postsynaptic cell type. *J. Neurosci.* **18**, pp. 10464–10472. (1998)

Nadasdy, Z. Hirase, H. Czurko, A. Csicsvari, J. Buzsaki, G., Replay and time compression of recurring spike sequences in the hippocampus. J Neurosci. 19, pp. 9497-9507 (1999)

Dave, A. S. and D. Margoliash. "Song replay during sleep and computational rules for sensorimotor vocal learning." Science **290**(5492): 812-816. (2000)

Foster, D. J. and M. A. Wilson. "Reverse replay of behavioural sequences in hippocampal place cells during the awake state." Nature **440**(7084): 680-3. (2006)

Louie, K. and M. A. Wilson. "Temporally structured replay of awake hippocampal

ensemble activity during rapid eye movement sleep." Neuron **29**(1): 145-156. (2001).

Felsen, G., J. Touryan, et al.. "Cortical sensitivity to visual features in natural scenes." PLoS Biol **3**(10): e342. (2005)

Sharpee, T. O., Sugihara, H., Kurgansky, A. V., Rebrik, S. P., Stryker, M. P., and Miller, K. D.. Adaptive filtering enhances information transmission in visual cortex. Nature *439*, 936-942. (2006)

Li, W., Piech, V., and Gilbert, C. D.. Perceptual learning and top-down influences in primary visual cortex. Nat Neurosci *7*, 651-657. (2004)

Fritz, J., Shamma, S., Elhilali, M., and Klein, D.. Rapid task-related plasticity of spectrotemporal receptive fields in primary auditory cortex. Nat Neurosci *6*, 1216-1223. (2003)

David, S. V., Vinje, W. E., and Gallant, J. L.. Natural stimulus statistics alter the receptive field structure of v1 neurons. J Neurosci *24*, 6991-7006. (2004)